A NOVEL COMPOSITE WITH NACREOUS DESIGNED TO RESIST WEAR AND CORROSION

A Thesis

by

YOUNTAE SHIN

Submitted to the Office of Graduate and Professional Studies of
Texas A&M University
in partial fulfillment of the requirements for the degree of

MASTER OF SCIENCE

Chair of Committee,	Hong Liang
Committee Members,	Alex Fang
	Partha Mukherjee
Head of Department,	Andreas Polycarpou

August 2014

Major Subject: Mechanical Engineering

ABSTRACT

This research explores new approaches in design and fabrication of novel composite materials in order to increase corrosion and wear resistance. By mimicking nature, nacreous particles from seashells were used as reinforcement in an aluminum matrix. Experimental approaches are used during investigation. A powder metallurgy process was developed to fabricate the nacreous-reinforced-aluminum matrix composites. Mechanical properties, corrosion and wear resistance were characterized through polarization technique, Vickers hardness and tribological tests. Experimental results showed that the corrosion resistance increases as the nacreous concentration increases. The hardness and wear resistance increased for up to 22% and 10% respectively due to the reinforcement effects of nacreous. With oxidation of aluminum during heat treatment, the mentioned properties were further improved for about 32 ~ 37%. This research is beneficial to develop novel material, which can be substituted the conventional composites.

DEDICATION

I would like to dedicate my thesis to my beloved wife, Suyeon for all of her love and support, and to my sweet and loving daughter, Mina.

ACKNOWLEDGEMENTS

I would like to thank my advisor: Dr. Hong Liang, and the committee members: Dr. Partha Mukherjee and Dr. Gwo-Ping Fang for their time and support to my research. I also wish to thank all surface science research group members for their advices in my research. I appreciate the Turbomachinery Laboratory at Texas A&M University, which provided fund for my research. I would like to thank Republic of Korea Army. Thank you for giving me the opportunity to study in the US.

TABLE OF CONTENTS

Page

LIST OF FIGURES

LIST OF TABLES

CHAPTER I

INTRODUCTION

This chapter consists of three major parts: the microstructures of seashells, aluminum matrix composites and their applications. Five different microstructures of seashells are briefly introduced. Among those, the microstructure of nacreous is explained in detail. The mechanical properties of the nacreous microstructure and the way of shell calcification are discussed. Some disadvantages of ceramic-reinforced aluminum composites are introduced. The application areas of the nacreous-reinforced composites are suggested in order to overcome the disadvantages of the ceramic-reinforced composites.

1.1. Lessons from nature

Nature has been undergoing evolutions since life has started on earth. All lives on earth have been adapting their biological characteristics to environments in order to survive. Understanding the biological characteristics in nature would provide us the guideline to excel in engineering.

Scientists are trying to develop new materials inspired by nature. There are lots of amazing things that humans can't even imagine or make. Figure 1 shows some examples of idea from nature. There is a small nerve-rich depression in front of snake's eye. The depression is called the pit [1]. The pit has a heat sensing system that allows snakes hunt warm blooded prey in the darkness. The beetle stenocara live in the desert. They collect water using a special feature of its back. The stenacara's back is covered by

many small bumps. The bumps are covered by wax except peaks that are wax free. This unique microstructure allows the stenacara to capture the water. The butterflies have a cooling system in the wings [1]. During flight, the heat is generated by friction of the wings and the sunlight. Generated heat is dispersed by the millions of thin film structures on their wings. The locusts travel in swarms of million but they never collide with others. The locust sends the signal out to other locusts to find their location, and change their moving direction before collision. Sharks' skin is covered with riblets that allow to moves efficiently in the sea. Sharks' skin reduces the water drag result from maintaining the water closer to the body. The chameleons can camouflage themselves with their chromatophore cells to match their surroundings [1].

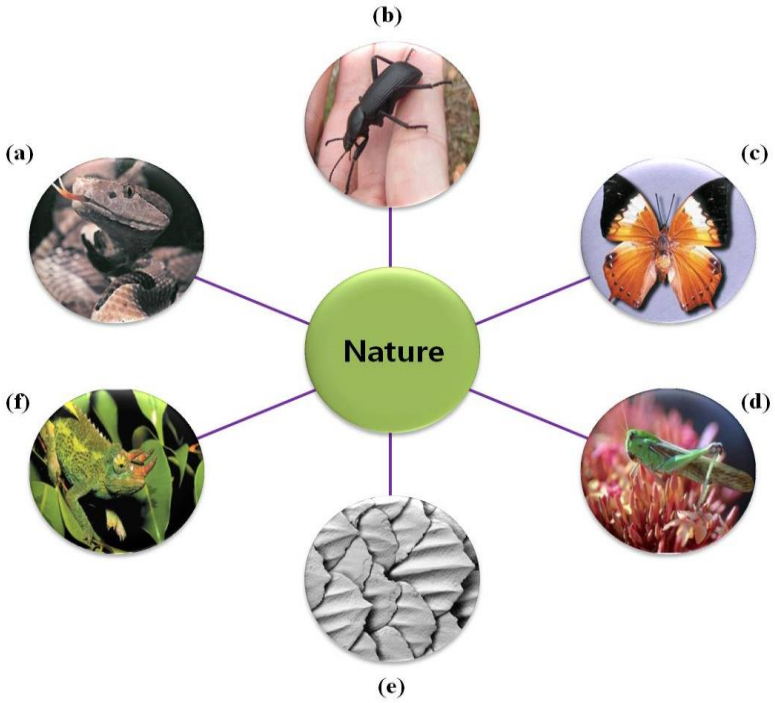

Figure 1. Examples of lessons from nature [1].

A marine mollusk builds a seashell to protect their soft body from a predator. Scientists divided mollusk species into 5 main classes (Figure 2): chitons, bivalves, scaphopods, gastropods and cephalopods [2]. Different environmental surroundings let the mollusk builds different types of the seashell [3].

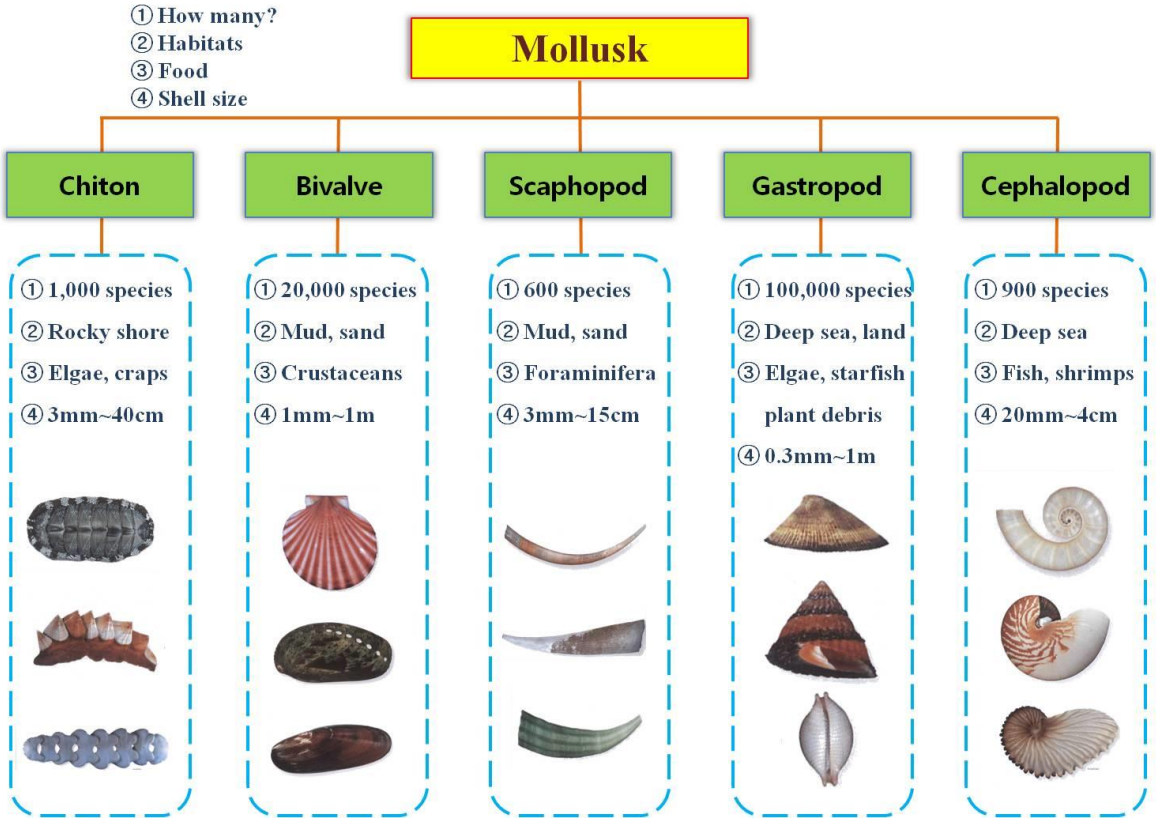

Figure 2. Five main mollusk classes [3].

There are approximately 1,000 chitons species. The chitons live on bottoms of the rocks on the rocky shore. They eat algae, bryozoans, foraminifera and some of chitons feed on small crustaceans. Some chitons can live as long as 25 years. A shell of

the chitons is linked with 8 shell plates. The seashell size varies from 3 mm to 40 cm [2, 3].

Approximately 20,000 bivalve species are living on earth. The bivalves are the second largest group from mollusks [2]. They live in from intertidal zone to the deep sea and most of them burrow in mud or sand. They feed on organic matter, algae, bacteria, small crustaceans and worms. The bivalves are enclosed by two symmetry valves. The left and right valves are laterally compressed and hinged by ligament. They open and close the shell with ligament and adductor muscle. One of the bivalves, the European panopea, is known as can live for 168 years [3]. In 2006, ocean scientist Paul butler found the 507 years old bivalves named Ming [4]. The size of seashell is range in from 1 mm to 1 m [3].

The scaphopods have about 600 species. They live buried in coral sand or muddy bottoms in the oceans from below the level of the tide to depth of 3000 ~ 6000 m. They eat the foraminifera. The shape of seashell looks like elephant tusks. The seashell size varies from 3 mm to 15 cm [3, 5, 6].

The gastropods are the largest group of mollusk with approximately 100,000 species. They are distributed in worldwide from the intertidal to the deepest trenches. Some live in fresh water, others live in terrestrial habitats such as mountains, forest and deserts. They feed on algae, corals, plant debris, blood of starfish and detritus. Some gastropods are known as can live for 30 years. They have asymmetrically coiled shell shape in right direction and some coiled shell become limpet like shape. The size of seashell is range in from 0.3 mm to 1 m [2, 3, 5].

There are 900 species of the cephalopods including cuttlefish and squid but only Nautilus species have external shell [3]. Nautilus species live in from shallow to deep water (10 ~ 1000 m). At night, they rise up to shallow water using eight arms to eat. They eat craps, fishes, shrimps, jellyfish and other mollusks [2, 3]. They have bilaterally symmetrical shell [2]. The shell size range is from 20 mm to 4 cm [3].

Seashells have been used for the purpose of decorations and some have been used for practical purpose. For example, several hundred years ago, Mayan implanted the piece of nacreous from seashells as a tooth [7]. Today, seashells' microstructures, especially nacreous microstructure, are widely studied due to their superior mechanical properties. Using biomimetic approaches, scientists are trying to mimic the nacreous microstructure with the expectation of fabricates a ductile ceramic [8, 9].

1.2. Seashells: the natural ceramic

1.2.1. Calcification

The molluscs have developed shells to support their internal organs and to protect their soft body from predators [7]. Biominerals and proteins are major components for formation of the shells [10]. The formation of the seashell is a biologically controlled mineralization process [7]. Figure 3 shows the typical seashell structure of a bivalve explaining the calcification process.

There are three components to be required for shell formation: an extrapallial space, a periostracum, and the calcifying matrix. In the extrapallial space, the shell calcification processing takes place. The periostracum support calcium carbonate crystals and seal the extrapallial space. The shell is formed by the matrix secreted from

mantle. The extrapallial space is the space for growth of the shell. This space is separated by shell, periostracum and mantle. The calcifying matrix contains proteins, chitin, polysaccharides and glycoproteins [7]. Calcium and carbonate are the most important ions to form the shell. The mollusc extracts the calcium and carbonate ions through the sea water and from the diets [11]. The organic matrices interact with the calcium and the carbonate ions and form the shell. The calcifying matrix is the key agent to nucleate the shell. The shapes, size and orientations of the shells are regulated by the matrix [7].

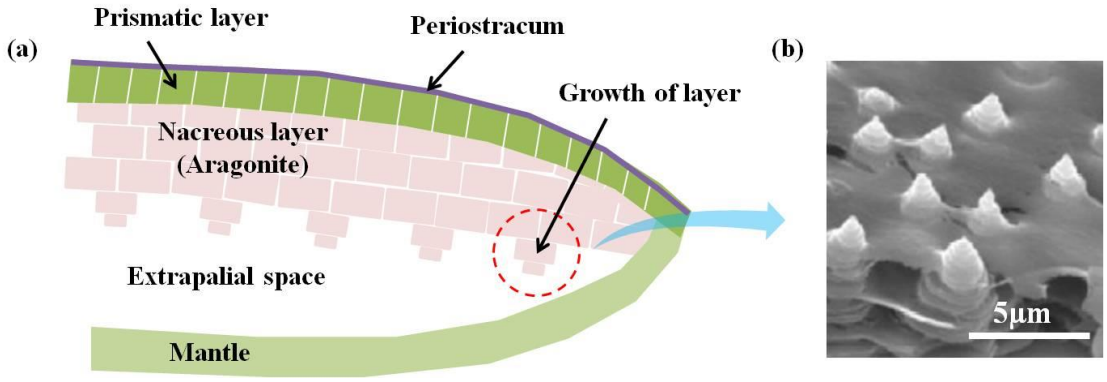

Figure 3. The typical mollusk shell structure [12].

The extrapallial space can be saturated because the periostracum seals the space. Thanks to this condition, calcium and bicarbonate ions are transported from the organ of mollusc. Calcium and carbonate ions are able to be stored as amorphous intracellular.

About 95 ~ 99% of shell is composed of $CaCO_3$ (calcium carbonate) and rest 1 ~ 5% is organic matrix. Calcified calcium carbonate layers are made of either calcite or aragonite and possess unique microstructures [7, 11].

1.2.2. Microstructures

There are tens of thousands seashell species on the earth, microstructure patterns of seashell can be categorized into five types of microstructures. Those are nacreous (also known as mother of pearl), prismatic, cross lamellar, foliated and homogeneous microstructures. Figure 4 shows different types of seashell microstructures. Not all seashells have only one microstructure. Some seashells have two different types of microstructure in the inner and outer layer of the shell [9]. For example, the bivalves like an abalone have prismatic (outer shell) and nacreous microstructure (inner shell) [7].

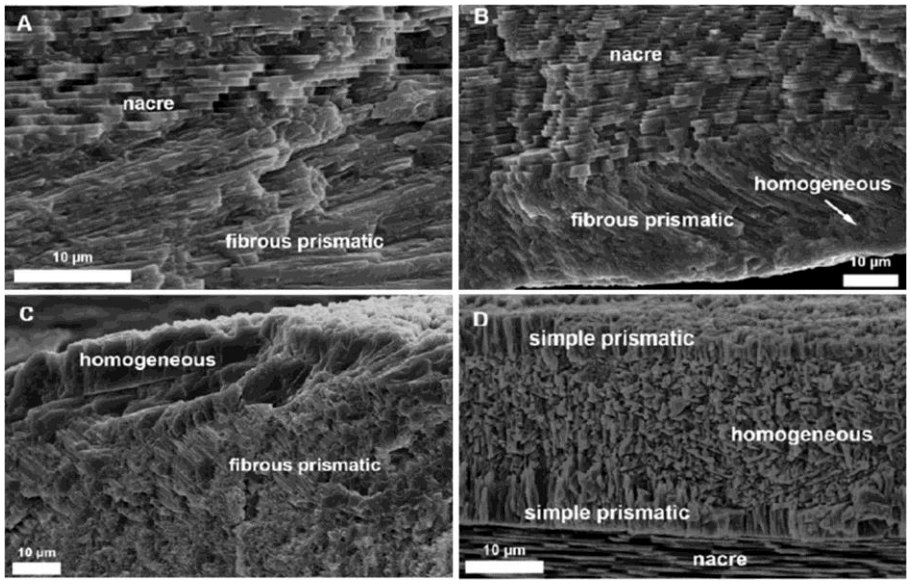

Figure 4. The different types of seashell microstructures [13]

Among microstructures of seashell, nacreous microstructure is widely studied due to good mechanical behavior. Table 1 indicates mechanical properties of microstructure of seashells. Cross lamella microstructure shows the highest hardness. However, nacreous microstructure has the highest toughness and good hardness.

Table 1. Mechanical properties of the seashell microstructure [9].

Microstructure	Mechanical properties				
	Tension (MPa)	Compression (MPa)	Flexural (MPa)	Stiffness (GPa)	Hardness (Vickers)
Nacreous	167	380	220	70	168
Prismatic	60	250	140	30	162
Cross-lamellar	40	250	100	60	250
Foliated	30	150	100	40	110
Homogeneous	30	250	80	60	

1.2.3. Nacreous microstructure

Nacreous microstructure is a composite with a brick and mortar architecture which consists of 95% calcium carbonate mineral layers and 5% organic matrix [8, 12]. Nacreous microstructure is shown in Figure 5. Nacreous shows the stacked calcium carbonate layers with 0.2 ~ 0.9 μm thickness and the thin organic matrix interlayer with 20 ~50 nm thickness. The calcium carbonate layer composed of polygonal platelets with 5 ~ 8 μm diameter and the organic matrix is filled in interlayer that plays a role as glue between the platelets [8, 12].

The brick and mortar architecture make the aragonite platelets harder and tougher. The platelets' surfaces are rough. The nanoscale mineral protrusions, called nanoasperities, are dispersed randomly on the platelets' surface [14]. The protrusions grew in the same crystal orientation (same c-axis orientation) as the platelets. When two mineral protrusions meet, they form a mineral bridge and the platelets become interlocked. The organic matrix contributes to nacreous toughness. During the mineralization process, each platelet is surrounded by the organic matrix and the interfaces of between platelets become soft. The protein in the interlayer adhered to the aragonite platelets. The protein can redirect the crack penetration path due to its soft and stretchable characteristics [8].

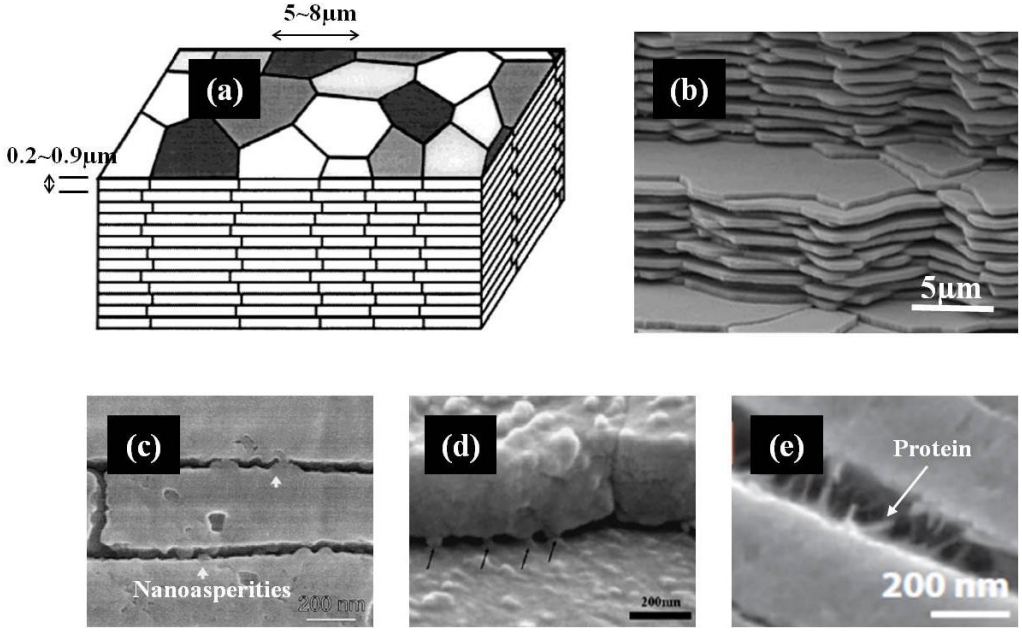

Figure 5. Nacreous microstructure [14].

Some scientist suggested replicating the nacreous microstructure with ceramics. A ceramic is hard but brittle. If ceramic has the nacreous microstructure, ceramic becomes hard and ductile. However, fabricating the nacreous microstructure with μm scale diameter and thickness is challenging. And achieving the strong bonding to attach the ceramics like protein is also challenging [8, 9].

1.3. Aluminum-matrix composites

1.3.1. The popularity of aluminum-matrix composites

Metal-matrix composite is a class of materials that consists metal and reinforcement in order to obtain desired mechanical properties [17, 18]. The matrix (metal) with good ductility and thermal conductivity is a softer phase. The reinforcement (fibers, plates, laminates, etc) with high stiffness and low thermal expansion is embedded in the matrix.

Aluminum matrix composite is the most popular metal matrix composite. The aluminum has low density (light weight), high corrosion resistance and the ability to be hardened by precipitation [18]. For those reasons, aluminum metal composites are widely used in aircraft industry, automotive, armors, electrical engineering and sporting goods [18, 19].

1.3.2. Reinforcements

Particles, dispersoids and fibres can be used as reinforcement in the aluminum matrix composites [19]. Volume fraction, grain size and distribution of the reinforced particles influence on the tribological behaviors and mechanical properties of the

material [20]. These factors can be controlled by selection of the reinforcing particles. To this end, the particle reinforcing method is popular [19].

Hard ceramic particles such as alumina and silicon carbide have been mostly used as reinforced particles in aluminum matrix composites [20]. There have been studies of aluminum matrix composites reinforced with alumina and silicon carbide to improve tribological behaviors since 1980s [21]. The addition of alumina and silicon carbide into aluminum alloy increase the wear resistance due to increased hardness [22]. A critical load had been reported to provide little improvement of wear resistance in ceramic reinforced aluminum matrix composite under dry sliding condition [21].

1.4. Application of nacreous reinforced aluminum matrix composites

Nacreous is a hard and tough natural ceramic. The aragonite has a similar density to aluminum (aragonite density: 2.83 g/cm^3 and aluminum is 2.7 g/cm^3). In addition, a seashell lives in the sea water containing 3.5wt% of NaCl without being corroded. Producing a material with nacreous microstructure is difficult due to the limitations of fabricating thin layers and weak adhesion. Nacreous particle can be used as the reinforcement in the aluminum-based composites.

The brake disc is mainly made of cast iron. REL.INC and Polytechnic Institute of New York University developed a prototype brake disc made of ceramic reinforced aluminum matrix composite in 2012. They are expecting that the brake disc of ceramic-reinforced-aluminum matrix will have 60% less weight (30 lbs from midsize sedans) and last three times longer than cast iron brake disc. They used conventional ceramics such as alumina (Al_2O_3) and silicon carbide (SiC) [23, 24].

Hard ceramic particles have some drawbacks. Hard ceramics are abrasive and brittle. Reinforcing a large portion of ceramic particles is restrained [25]. Sometimes hard ceramics increase the wear volume loss of counter face because of their abrasive action [21]. While braking, the surface of the brake disc contact with the surface of the brake pad. In short, the counter face needs to be considered to design the brake disc.

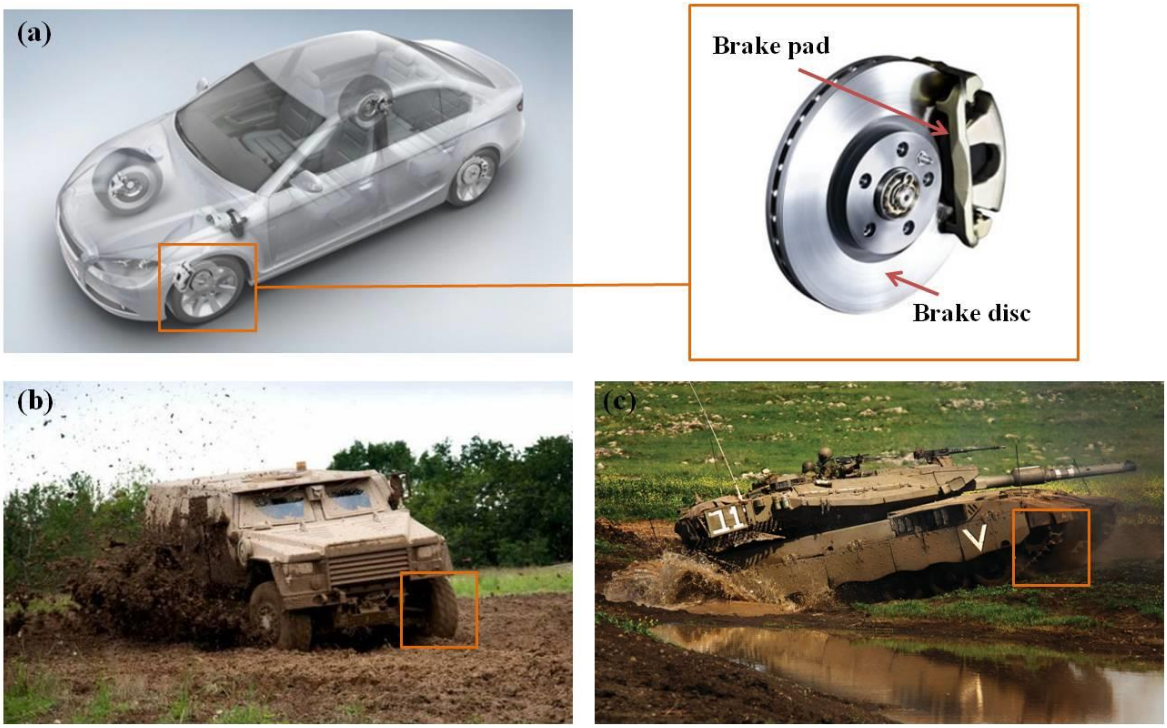

Figure 6. Possible applications of nacre-aluminum composites [29].

Nacreous-reinforced-aluminum matrix composites will be able to substitute the conventional brake disc. Nacreous has good hardness, toughness and potential in high corrosion resistance. Nacreous is even lighter than Al_2O_3 (3.95 g/cm^3) and SiC (3.21 g/cm^3). As well as brake disc, nacreous can be used in the areas of the military armored vehicles which require wear, corrosion resistance and light weight. It is hypothesized that they would be able to accomplish the mission for a longer time under extreme weather conditions with high mobility.

1.5. Principles of enhancement in particle-reinforced composites

A composite material is composed of two or more physically and/or chemically distinct phase: matrix phase and dispersed phase [30]. The reinforced particles are dispersed phase. The characteristics of the reinforce particles such as concentration, size, shape, distribution and orientation influence on both hardness and wear resistance [31, 32].

Small and well distributed particle increases the hardness [31]. A small-grained material is harder than bigger-grained material because they have more grain boundaries. The grain boundary is a barrier of the dislocation motion during plastic deformation. When the dislocation encounters the grain boundary, the dislocation must change the direction of movement. This mechanism is expressed as Hall-Petch equation (σ_y: yield strength, σ_0, K_y: constants, d: grain size)

$$\sigma_y = \sigma_0 + \frac{k_y}{\sqrt{d}}$$

Higher particle volume fraction increases the hardness. The rule of mixtures equation for increasing the hardness as follows (H: hardness, V: volume fraction, c,r,m: composite) [32, 33]

$$H_c = V_r H_r + H_m V_m$$

There are some intrinsic factors to affect wear resistance. Those are hardness, volume fraction and interfacial bonding [32]. Most of all, the higher hardness increase the wear resistance. This relationship is shown in Figure 7.

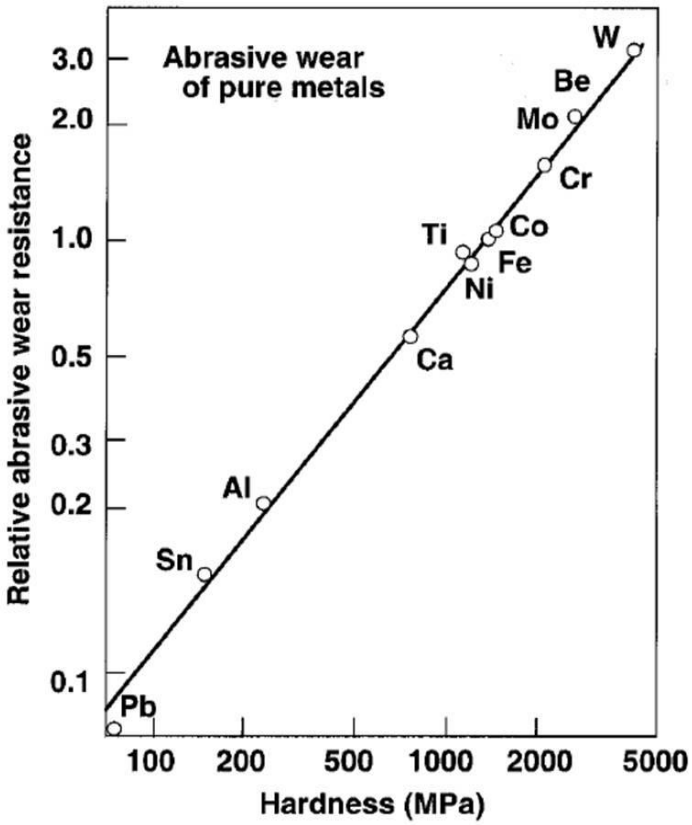

Figure 7. The relationship between hardness and wear resistance [34].

According to the discussion above, the wear resistance can be increased by adding the higher volume fraction of reinforcements. In case of metal-matrix composite, as much as 70% of ceramic particles can be used as reinforcement [32]. As the volume fraction of ceramic particles increases, the wear volume losses of counter face material increases [21, 32].

Good interfacial bonding increases the wear resistance. Poor interfacial bonding tends to pull out the particles from the composites during the wear test [32]. This means that reinforced particles are pulled out resulting weakened matrix.

In summary, this chapter discussed the effects of nacreous particles on aluminum matrix. Mimicking nature, this research develops a novel composite with high wear and corrosion resistance using seashell as reinforcement. The following chapters are including motivation and objectives, experimental approaches, effects of the nacreous on corrosion protection and tribological performance. Mechanisms of the reinforcement will be discussed in corresponding chapters.

CHAPTER II

MOTIVATION AND OBJECTIVES

As discussed in the Chapter I, the aluminum–matrix-composite brake disc weighs approximately 60% as much as a cast iron brake disc. Hard ceramic particles can be used as reinforcement in the aluminum-matrix composites. The main issue is the abrasiveness and brittleness of the ceramic particles that might affect the wear resistant resulting the wear and total volume loss. The nacreous microstructures have potential to increase wear resistance due to their unique microstructure. Those are also lighter than conventional ceramics. Using nacreous as reinforcement particles could have several advantages. For example, a brake disc made of nacreous-reinforced-aluminum composites could increase the material's lifespan as well as reduce the weight of the vehicles.

The objectives of this research are to:

1. Developing novel composite materials containing nacreous.
2. Obtaining high wear and corrosion resistance in those materials.
3. Obtaining understanding in effects of components on tribological and electrochemical performance

The ultimate goal of this research is to establish the relationship of process-property of the nacreous-reinforced-aluminum composites. Potential applications of the novel materials will be explored. Through this research, the durability for brake disc can be improved.

This research uses experimental approach and characterization techniques are listed in the following. The nacreous will be obtained from natural seashell and crashed into the powder. Nacreous-reinforced-aluminum composites will be made through the powder metallurgy process. The Vickers hardness tester will obtain the hardness values of the specimens. The morphology of the nacreous powder will be studied with scanning electron microscope (SEM). The image analyzing software and water displacement method will be used to measure the porosity. The energy-dispersive X-ray spectroscopy (EDS) will be used to understand the chemical reactions or microstructures in the composites. The potential dynamic test and pin-on-disc wear tests will be conducted in order to evaluate tribological and corrosive behavior.

The following chapters discuss the experimental results and discussions. Chapter IV discusses the effects of the nacreous on corrosion resistance. The corrosion mechanism of nacreous-reinforced composites will be analyzed via observation of surfaces with SEM and optical microscope. Chapter V discusses the effects of the nacreous on tribological performance in terms of wear.

CHAPTER III

EXPERIMENTAL PROCEDURE

This chapter contains experimental procedures to be followed to accomplish this study. It consists of several sections; materials, powder metallurgy process, and evaluation methods. The trochus seashell with nacreous microstructure was used for this study. The powder metallurgy process was conducted to fabricate the nacreous-reinforced aluminum matrix composites. The Vickers hardness tester, pin-on-disc tribometer and Gamry instrument were used to evaluate the hardness, wear and corrosion resistance. The surface of the each specimen was analyzed under scanning electron microscope (SEM), optical microscope, and profilometer.

3.1. Materials

3.1.1. Sample seashell

Natural trochus seashells were purchased from a local store (Hobby Lobby, COLLEGE STATION, TX). Trochus seashell has a prismatic microstructure on the outside and a nacreous microstructure on the inside. Typically, prismatic and nacreous microstructures show similar Vickers hardness numbers but nacreous has much higher toughness. The size of the trochus seashell was approximately 6 cm in height and 5 cm in width, as shown in Figure 8 in SEM images. The details about SEM procedure will be discussed later in thischapter. Here the left figure of the natural seashell. The right figure shows nacreous layers of the trochus seashell. The layered structure is of interested.

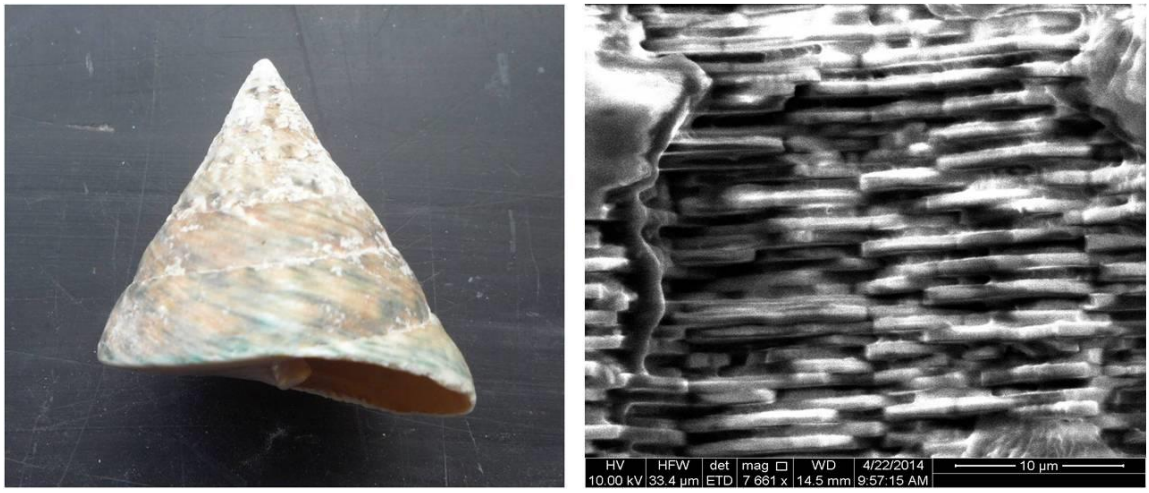

Figure 8. The nacreous microstructure of the top shell

3.1.2. Nacreous powder

The sample seashell (trochus) has two types of microstructure. One is a nacreous and another is a prismatic microstructure. The nacreous was used in this study. The nacreous microstructure consists of 95% aragonite ($CaCO_3$) crystals and 5 % of nacreous [7]. The aragonite has a density of 2.83 g/cm^3 and a melting temperature of 825 ℃.

Pure pearly layers of inner shell with a nacreous microstructure were separated from an outer shell with a prismatic microstructure. To take pure nacreous shells off, seashells were crushed and split by a hammer and a flat headed driver. The thickness of the nacreous layer was in a range of 0.52 mm ~ 0.99 mm. Pure nacreous shells were cleaned with a liquid soap and acetone to remove mud. The nacreous flakes were ground with a mortar and pestle to make it into powder. The seashell powder was filtered by a sieve with 53μm mesh size.

3.1.3. Aluminum powder

Aluminum (Al) powder with a density of 2.7 g/cm^3 and a melting temperature of 660.32 °C was used as a metal matrix. The Al powder (>99% purity) was purchased from Vlaimet Inc.

3.1.4. Copper (II) oxide powder

The 7.9 wt. % of copper (II) oxide (CuO) powder with a density of 6.31 g/cm^3 and a melting temperature of 1,336 ℃ was added to the matrix in order to increase hardness. Based on nominal compositions of wrought Al alloy 2000 series (Table 2), 6.3 wt. % of copper and 1.6 wt. % oxygen were added [33]. The CuO powder (>99% purity) was purchased from Sigma - Aldrich.

Table 2. Nominal compositions of wrought aluminum alloy 2000 series

	Percent of alloying elements					
Alloy	Silicon	Copper	Manganese	Magnesium	Nickel	Titanium
2008	0.65	0.9		0.38		
2018		4.0		0.7	2.0	
2024		4.4	0.6	1.5		
2036		2.6	0.25	0.45		
2117		2.6		0.35		
2219		6.3	0.3			0.15

3.2. Powder metallurgy process

3.2.1. Mixing

Different weight percentages of nacreous powder (0, 1, 2 and 5 wt. %) were added to the Al and CuO-Al composite to evaluate the effect of nacreous on hardness, wear and corrosion. Table 3 shows the concentration of the elements in prepared specimens. Different types of powders were mixed together for 3 hours using the rotating mixer.

Table 3. Percentage of powder in prepared specimen

	Weight percentage of powder in prepared specimens							
Powder	1	2	3	4	5**	6**	7**	8**
Nacreous		1.0	2.0	5.0		1.0	2.0	5.0
Aluminum	100	99.0	98.0	95.0	92.1	91.1	90.1	87.1
Copper					6.3	6.3	6.3	6.3
Oxygen					1.6	1.6	1.6	1.6

** Specimen 5~8 were prepared 2 for each.

3.2.2. Pressing

Powder pressing is a straight forward method to compact powders into solid parts. To form solid parts called green compacts from powders, the compaction technique with punch and die was used at room temperature. The word green means that the compact has not yet sintered [34, 35].

Compressibility is defined as the ability of powders to form a green compact during the die compressing process. Having a higher compressibility means having a higher possibility to be compacted with a higher density [35]. During the compressing process, the powders fill in the spaces between powder particles. Particle shape and size have an effect on compressibility. Typically, spherical and small particles can occupy more spaces [35]. In other words, the density of the green compact (green density) increases when powders have a spherical shape and smaller particles.

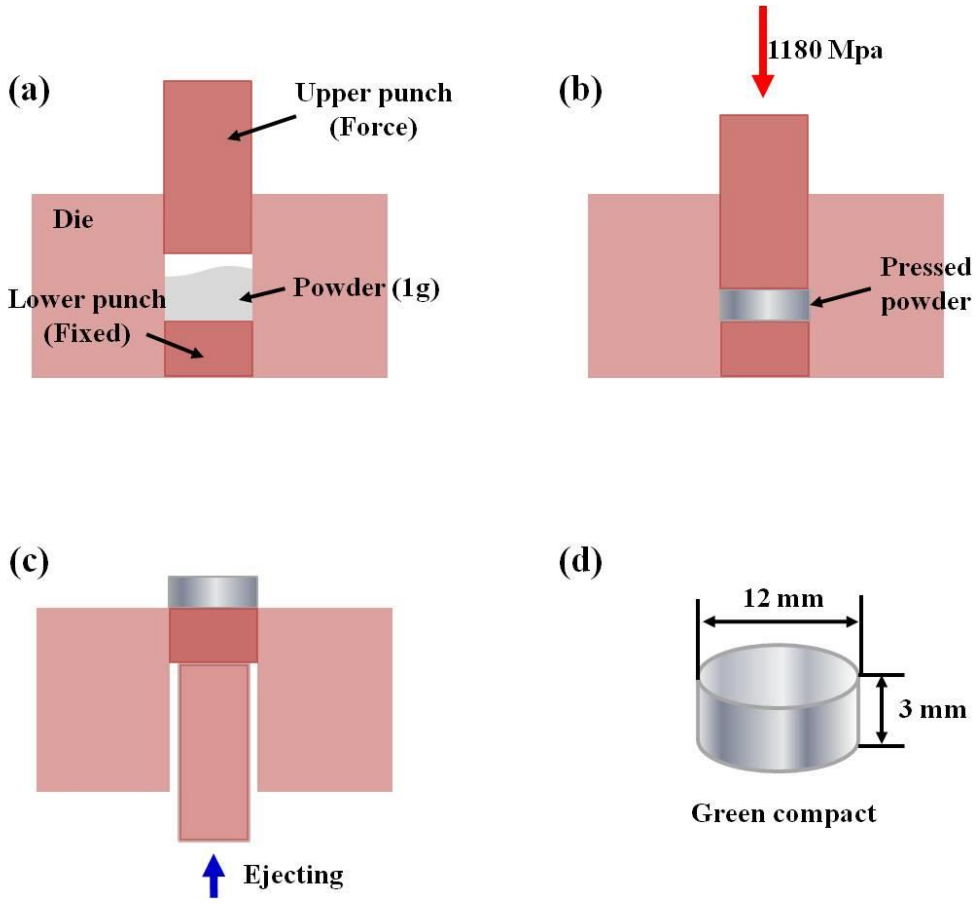

Figure 9. Powder pressing procedure.

For each powder pressing, 1 g of mixed powder was poured into the die cavity with a diameter of 12 mm and length of 3 cm. The circular bars were used as a punch. The die and punch were made from the steel. The compressing equipment (Midvale-happenstall Co.) which can put load up to 40000 lbs, was used as a compaction machine to produce green compacts.

Circular specimens were pressed with 1180 Mpa for the mixed powders. The resultant thickness of green compacts was approximately 3 mm. The procedure of powder pressing is shown in Figure 9.

In the green compact, density is not uniform. The mechanical properties vary across the volume of the green compact and depend upon compaction pressure. Therefore, the final green compact will still has porosity and the true density is higher than the green density [34].

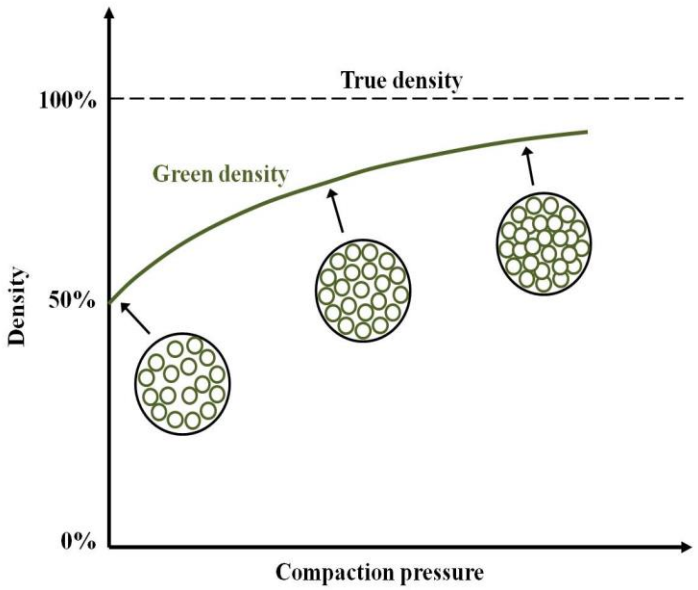

Figure 10. The relationship between green density and true density [34].

3.2.3. Sintering

The green density of the specimens can be increased by a sintering process. Sintering is a heating process to reduce the porosity of the bulk volume by a diffusion mechanism. The sintering temperature is typically two thirds of the melting point (rule of thumb) of the material. During heating, the pores shrink and the powder grain forms as a mass [29]. Conventional sintering will reduce the porosity, but will not eliminate all the porosity. Figure 11 shows diagram of the sintering mechanism.

3.

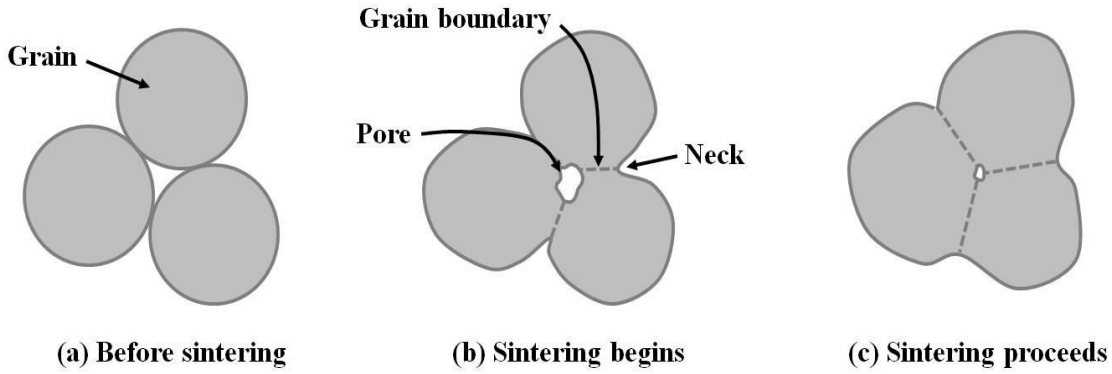

Figure 11. Sintering process [29].

Sintering was conducted by the tube furnace (Thermo Electron Corporation). The nacre-Al composites were sintered at 440 ℃ for 6 hours. In the case of the nacre-CuO-Al composites, two different sintering temperatures and times were applied. One group of the nacre-CuO-Al composite was heated to 440 ℃ for 6 hours, and the other nacre-CuO-Al composite was heated to 500 ℃ for 0.5 hours.

3.3. Corrosion test

3.3.1. Polarization technique

Most metals corrode at the interface between the metal surface and the electrolyte solution through electrochemical reaction [38]. The corrosion process is the combination of oxidation and reduction. [29]. Corrosion typically happens at an equilibrium point determined by opposing electrochemical reactions, the anodic and cathodic reaction. Oxidation takes place in anodic reaction and reduction takes place in cathodic reaction [38].

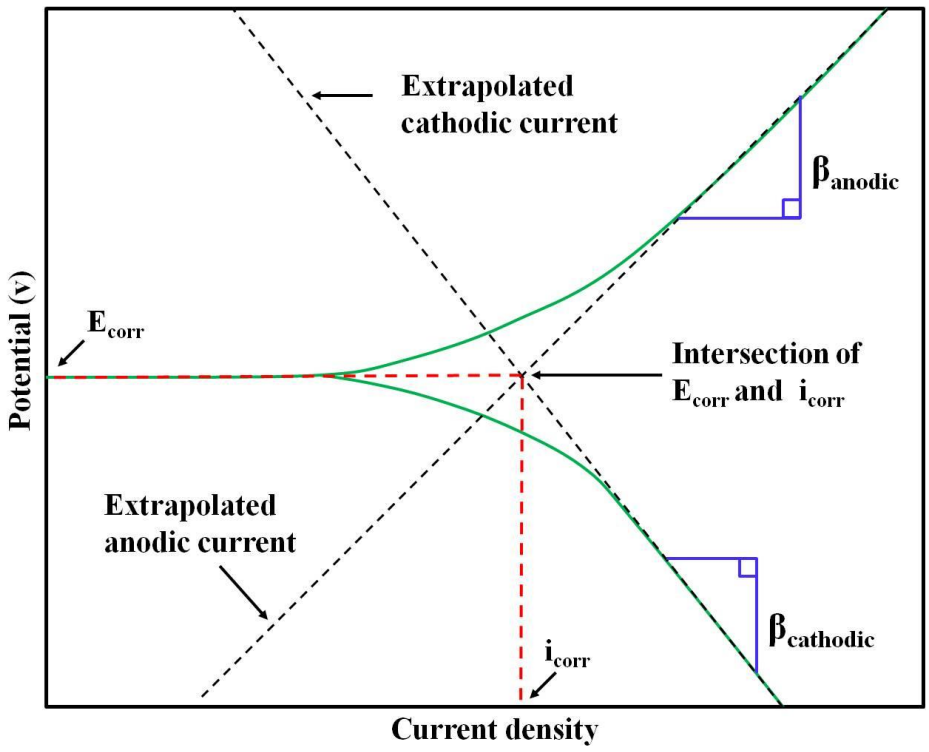

Figure 12. The normal metal polarization curve during corrosion process.

The electrochemical reactions follow Faraday's law: the amount of material from oxidation-reduction reaction is proportional to the amount of passed current flux. The polarization resistance technique is one of the most useful techniques for determining the corrosion rate [39].

The corrosion rate can be calculated from establishing the slopes which are known as Tafel slope extrapolation. [40]. Figure 12 illustrates a normal metal polarization curve during corrosion process.

In Figure 12, the dashed black lines are the theoretical current for the anodic and cathodic reactions. The curved green lines are the sum of measured current for the anodic and cathodic reactions. Calculation of penetration corrosion rate (CR) can be expressed as follows:

$$CR = I_{corr} \frac{KEW}{\rho A}$$

where I_{corr} is a total anodic corrosion current (μA), ρ is density in g/cm^3 , A is sample area in cm^2, K is a constant, and EW is the equivalent weight in g/equivalent [38, 41]. The constant K depends on units for corrosion rate (Table 4). In this equation, if I_{corr} is measured, corrosion rate can be calculated. However, I_{corr} cannot be measured directly from polarization curve.

Table 4. Units for penetration corrosion rate (CR) [41]

	Units			
CR	I_{corr}	ρ	K	Units of K
Mpy	$\mu A/cm^2$	g/cm^3	0.1288	mpy g/μA
mm/yr	A/m^2	kg/cm^3	327.2	Mm kg/A m y
mm/yr	$\mu A/cm^2$	g/cm^3	3.27×10^3	Mm g/μA cm y

The start point to measure I_{corr} is from the Tafel equation: where the current density $\eta = E_{applied} - E_{open\ circuit}$, β is the Tafel slope, i_0 is the exchange current density and i is the applied current density.

$$\eta = \beta \log \frac{i}{i_0}$$

Therefore, the Tafel slopes can be established from the linear sections on the polarization curve. The equilibrium point of the anodic and cathodic reaction can be extrapolated from the Tafel slopes. At the equilibrium point, the potential is the corrosion potential, E_{corr} and the anodic corrosion current (i_{corr}) can be obtained. [42].

3.3.2. Corrosion test procedure

The potential dynamic test was performed using a Gamry instrument REF 600 to measure the corrosion resistance. The applied voltage range was -1.2 ~ 0.3V. Anodic and cathodic polarization curves were drawn with a scan rate of 20 mV/s. The exposed area of the specimens was 0.567 cm^2. 3.5 wt% of sodium chloride (NaCl) in deionized (DI) water was used as a solution. The Gamry instrument is illustrated in Figure 13.

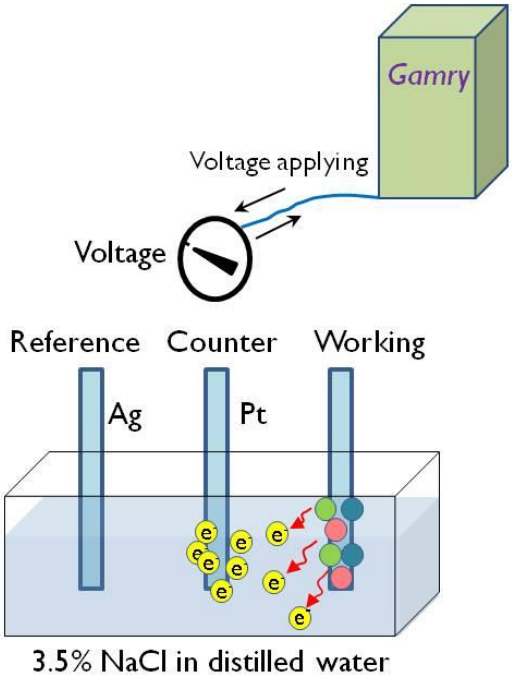

Figure 13. The gamry instrument.

3.4. Hardness test

3.4.1. Vickers hardness tester

Vickers hardness tester is mostly used to measure the hardness of small parts, thin sections and selected surface areas. The diamond indenter has the pyramid shape with 136° angle of opposing 4 indenter faces. To measure the hardness, the square based pyramidal shaped diamond indenter is moved down under an applied load ranging between from 1 to 120 kgf. After the indenter ceases the further penetration, the force remains for 10 to 15 seconds. The diagonals of the permanent impression are observed under a microscope and measured. The illustration of the Vickers indentation is shown

in Figure 14. The Vickers hardness number is calculated from the following equation where P is load and d is diagonal [29, 36].

$$HV = \frac{2P\sin(136/2)}{d^2} = \frac{1.8544P}{d^2}$$

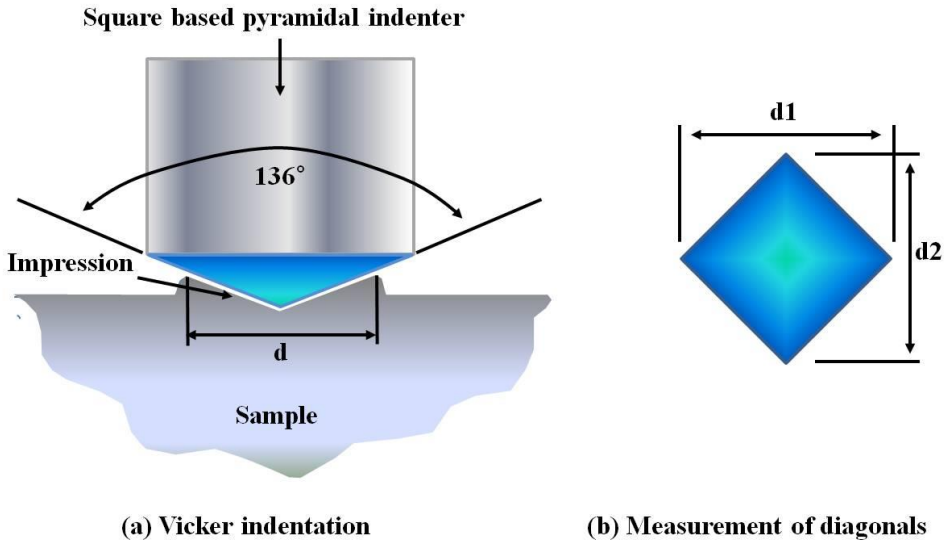

Figure 14. The Vickers hardness tester.

3.4.2. Hardness test procedure

Before each test, a polishing process was performed to avoid errors and to obtain constant values. The surface of the samples was polished on 3 different grinding papers of 800, 2400 and 4000 for 4 minutes, successively.

The hardness test was conducted with the Vickers hardness tester (LM 300 AT, LECO Co.). Uneven surface status of the specimen was considered. Total 10 dispersed

impressions were made over the surface of the each specimen. The length of the diagonals was measured using a digital measuring eyepiece on the main body of the Vickers hardness tester.

3.5. Wear test

3.5.1. Pin-on-disc tribometer

A pin-on-disc tribometer is suited for measuring coefficient of friction and wear rate. The pin on disc tribometer was named due to the testing method using a pin and a disc. The pin is loaded under an applied force onto the sample on a rotating disc.

The friction force sensor measures the deflection of the elastic arm during the experiment. The friction coefficient (μ) is calculated with the following equation where N is the normal force.

$$F = \mu N$$

Wear rate for the materials is determined by the volume loss rate of the materials during the test [37].

3.5.2. Wear test procedure

The wear test was carried out using a pin-on-disc tribometer (linear reciprocating mode) from CSM instrument (TRB series). Figure 15 shows the pin on disk linear mode used for this study. The wear test was performed under 2N normal load at an indoor atmospheric condition. A sliding distance was 2.8 m with 1 cm/s sliding speed. The length of the wear track was 2mm. No lubricant was added during the tests.

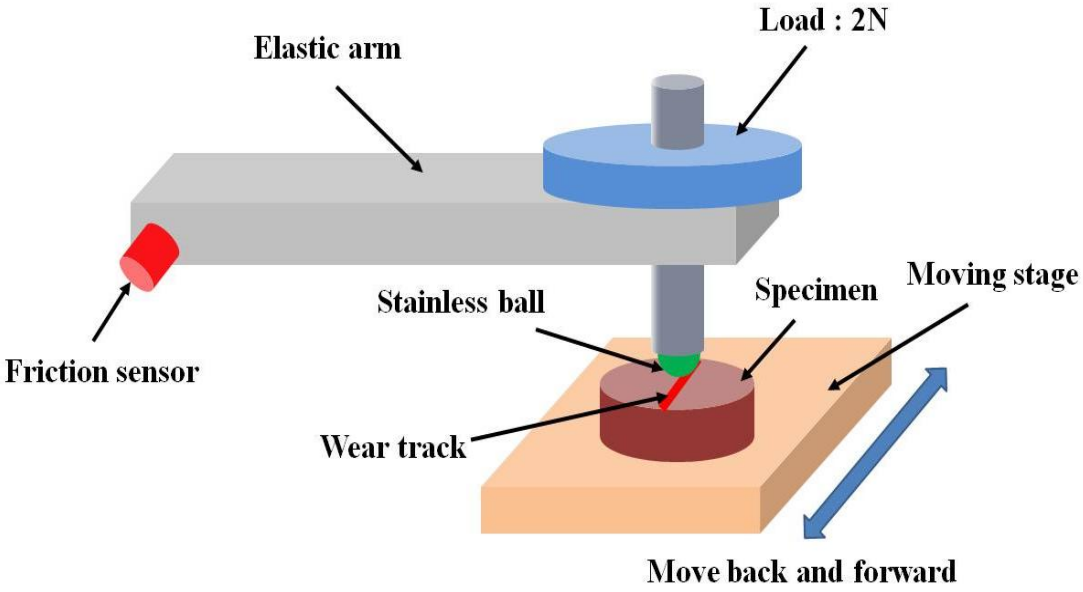

Figure 15. The pin-on-disc tribometer.

3.6. Characterization

3.6.1. Wear volume loss measurement

After the pin-on-disc wear test, the wear tracks were analyzed using a profilometer (P-6, KLA Tencor). The profilometer provides the morphology of the wear tracks shown in Figure 16. The width and depth of the wear tracks were obtained from the profilometer and wear volume losses were calculated.

$$\text{Wear volume loss} = \text{Width} \times \text{Depth} \times \text{Length}$$

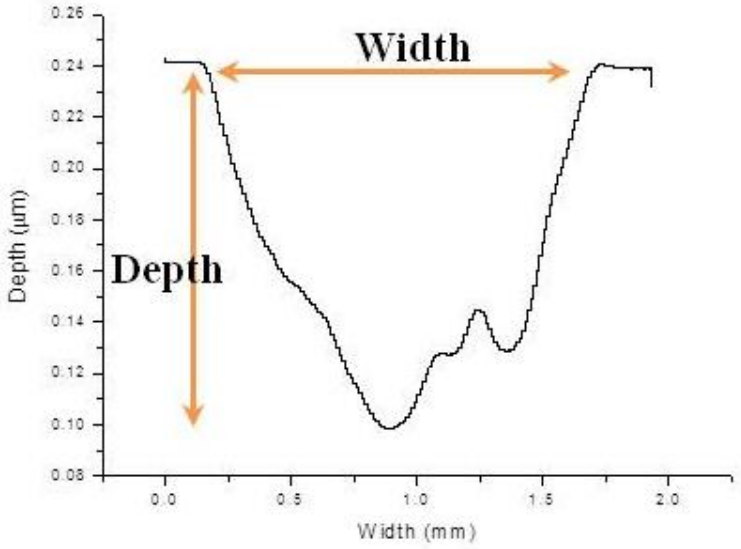

Figure 16. Obtained morphology of the wear track by the profilometer.

3.6.2. Porosity measurement

The porosity of specimens was measured by the software named ImageJ and the water displacement method. To compare the porosity in nacreous contained composites, surface images were taken by optical microscope. The area distributions of the pores were analyzed, and the porosity of the surfaces was calculated by ImageJ. The process of the surface porosity measurement is shown in Figure 17. The bulk porosity was measured in order to compare the porosity between the Al and the CuO-Al composites by the water displacement method. Before the measurement, specimens were immersed in the distilled water for 6 hours.

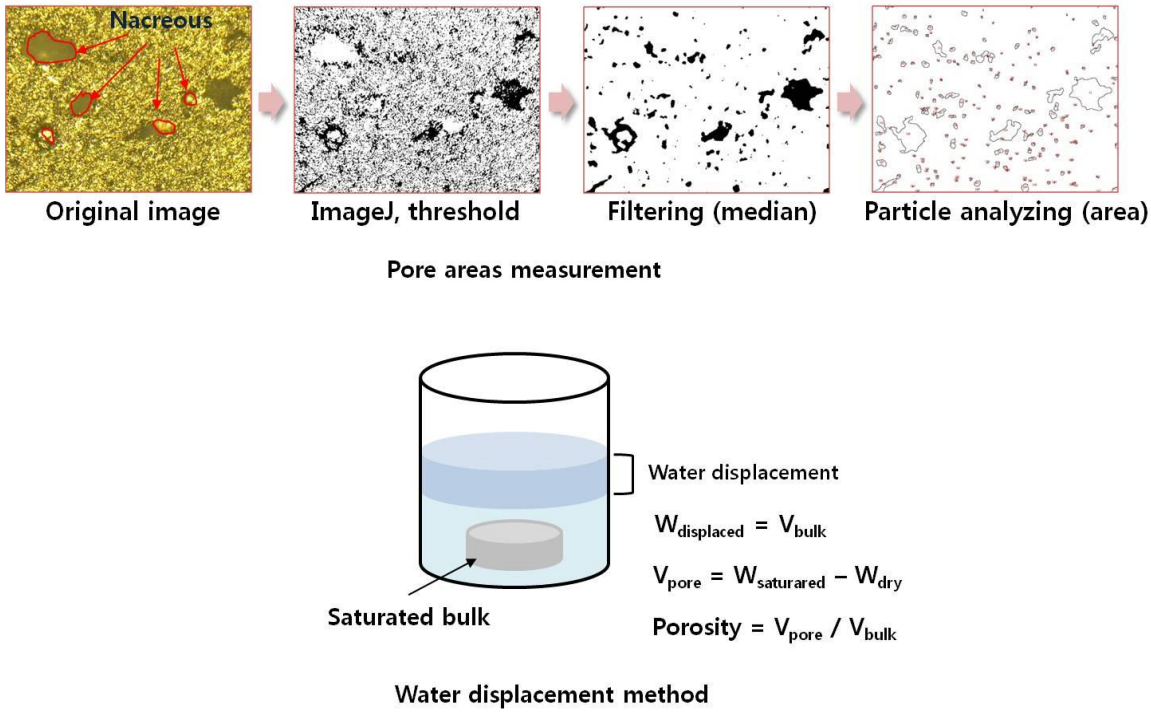

Figure 17. Porosity measurements.

3.6.3. Microscopic analysis

The optical microscope (VHX-600, Keyence) was used to analyze the surface pores and corroded surfaces. Pores on the surface, types of wear mechanisms, and the morphology of the nacreous particles after corrosion process were observed from the optical microscope images. Images were taken using 300x, 500x and 700x magnification.

Two different types of SEM were used for further analysis of the surfaces. Wear mechanisms and corrosion mechanisms were effectively analyzed by the Vega II LSU SEM (Tescan). In the range of 5kV ~ 10kV energy of beam was used. Applied working distance was about 20 ~ 33mm. The image of the nacreous microstructure in the top shell and EDS mapping images were taken by the Quanta 600 FE SEM (FEI).

CHAPTER IV

CORROSION PROTECTION

This chapter discusses the effects of nacreous particles on corrosion. Due to the existence of porosity, it is firstly discussed in terms of defects on corrosion protection. Secondly, the polarization experiments were conducted to measure the corrosion rate. Next, the types of corrosion are analyzed based on the images of SEM and optical microscope. Finally, the relationship between nacreous and corrosion mechanism are discussed.

4.1. Porosity

Porosity influences on the corrosion resistance. Nacreous powders would not have spherical shape because nacreous powders were produced by a pestle and mortar with bare hands. Addition of the nacreous powders may cause the pores in the specimens due to their irregular shapes and sizes. The porosity was measured using the software ImageJ and water displacement method. Pores are observed around nacreous grain (Figure 18). Nacreous grains have larger size than matrix and have irregular polygonal shape. Porosity could be one of the reasons to affect corrosion. More pores allow more areas to be attacked from Cl^- ions. The porosity was measured using the software named ImageJ and the water displacement method.

Figure 18 shows the mapping images of pores on the surface from optical microscope images. The 0, 1, 2 and 5 wt% nacre-Al composites show that the percentages of pore areas on the surface are 0.21%, 0.34%, 0.51% and 1.20%,

respectively. The measured bulk porosity from the water displacement method shows CuO-Al composites have less porosity than Al (Figure 19).

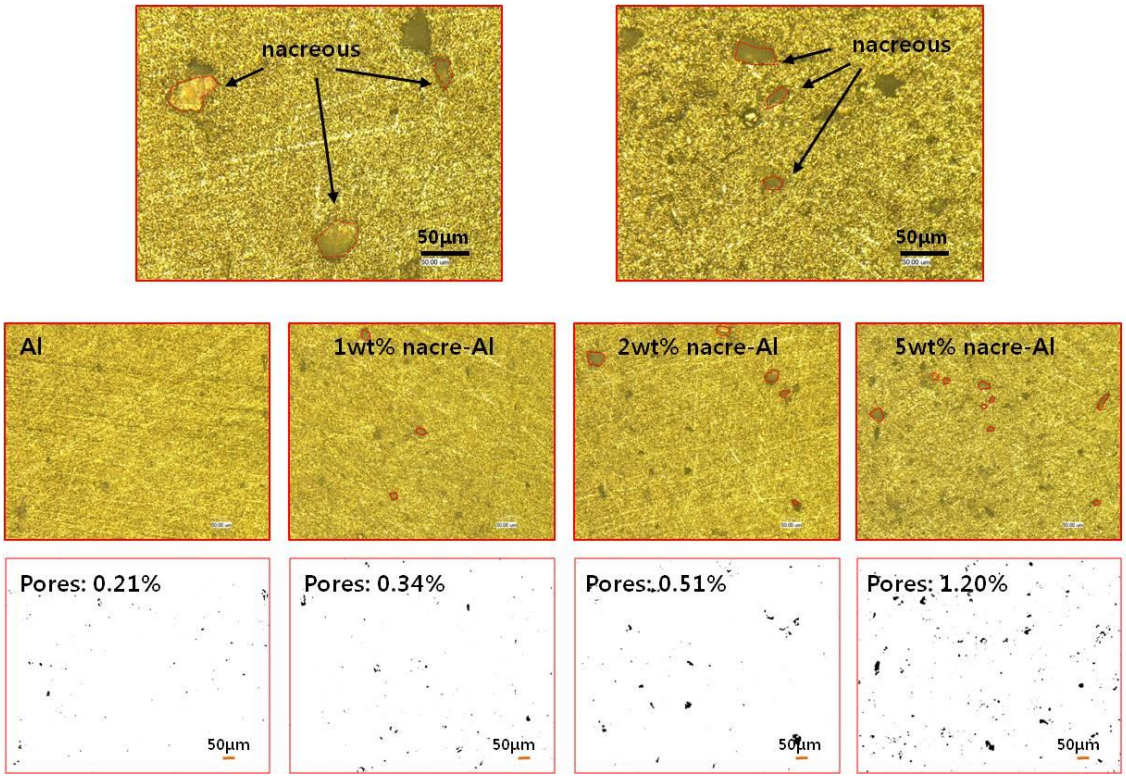

Figure 18. Surface porosity analysis.

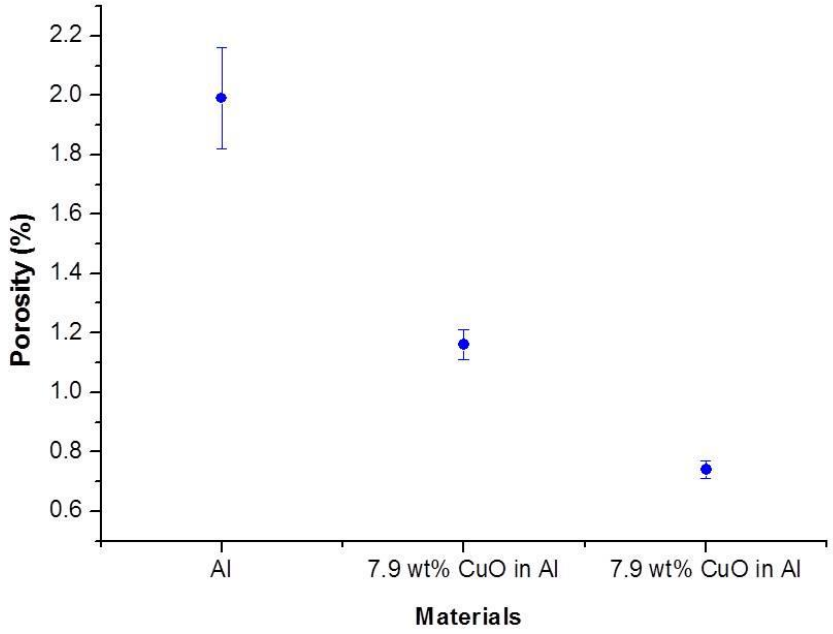

Figure 19. Measured bulk porosity.

4.2. Corrosion rate

Tafel slopes were established on the polarization curves in order to obtain the anodic corrosion current (I_{corr}). The calculated corrosion rates are listed in Table 5.

Figure .(a) is the polarization curve of the nacre-Al composites. The addition of the nacreous particles decreases the corrosion rate. 1wt% nacre-Al composite shows the lowest corrosion rate between specimens. As the nacreous concentration increases, the corrosion rate goes up more.

This phenomenon can be observed in CuO-Al composites (sintered at 440°C for 6H). In Figure .(b), 1wt% nacre in CuO-Al composite shows much lower anodic

corrosion current than the others. Like the nacre-Al composite, the corrosion rate goes up more in 2 and 5wt% nacre -CuO-Al composites.

As nacreous concentration increases, the porosity increases. The porosity could be a reason that 2 and 5 wt% nacre concentration show higher corrosion rate than 1 wt% nacre concentration. This means that nacre can protect the matrix from corrosion, but the porosity should be considered to obtain the best corrosion resistance. From the results of the Nacre-CuO-Al composites' corrosion test, the importance of porosity control is clearly shown. In Figure (b), the corrosion resistance of 1wt% nacre-CuO-Al composite was highly increased compare to 1wt% nacre-Al composite. This may caused by the oxygen from CuO during the sintering. As the reduction takes place on CuO grain, oxygen is released from CuO grain. The oxygen may occupy the adjacent pore and reduces the porosity of the matrix.

Nacreous embedded CuO-Al composites which sintered at 500°C for 0.5 hours show higher anodic corrosion current than CuO-Al composites in Figure .(c). Unlike Al and CuO-Al (sintered at 440°C for 6H) composites, nacreous caused higher corrosion rate in the composites. These composites were undergone 30 minutes heating time during sintering. Composites would have more defects result from shorter heating time. The defects are weak against Cl ions attack. The defects may the reason that why the corrosion resistance decreased in the composites.

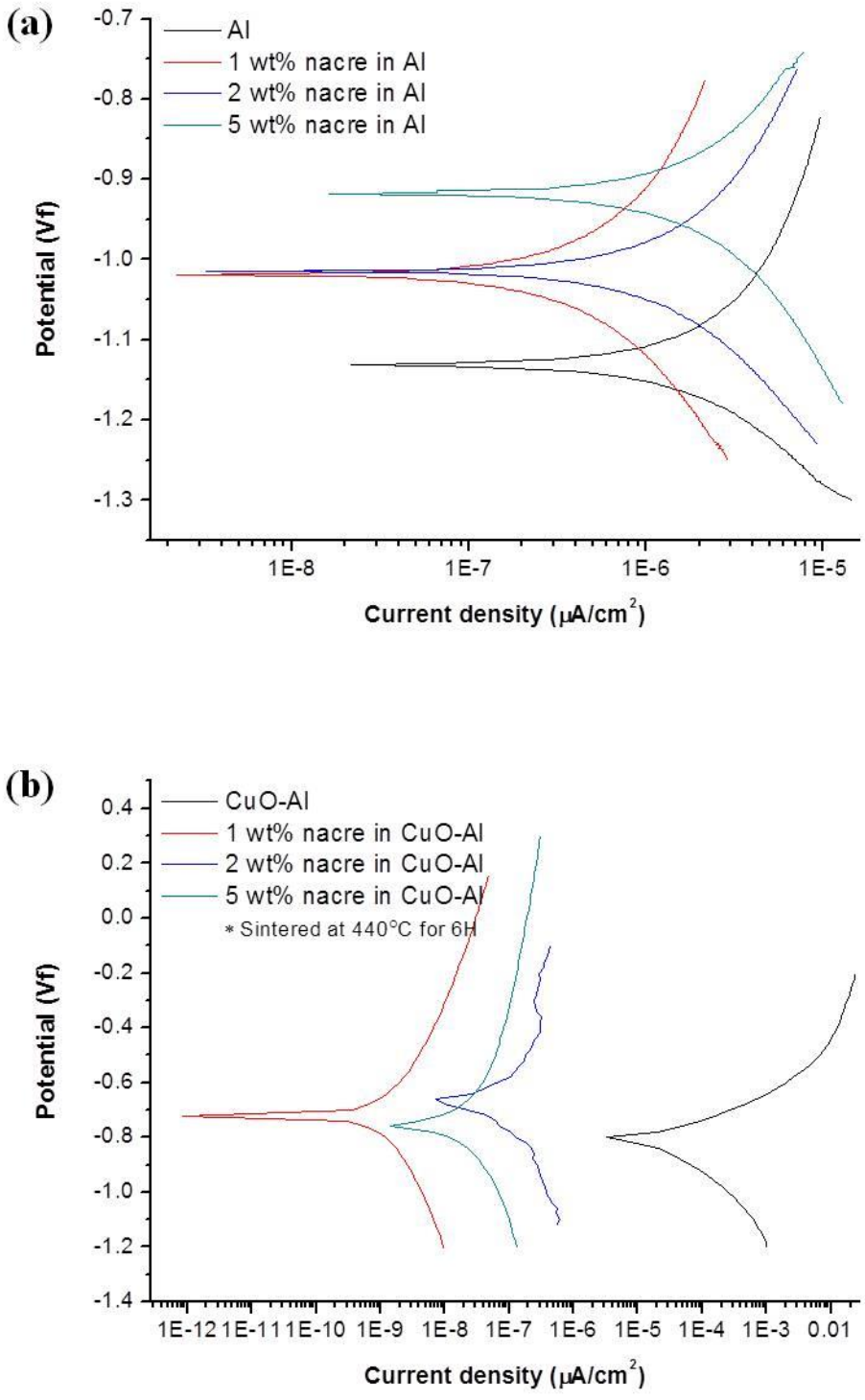

Figure 20. Polarization curves of the specimen.

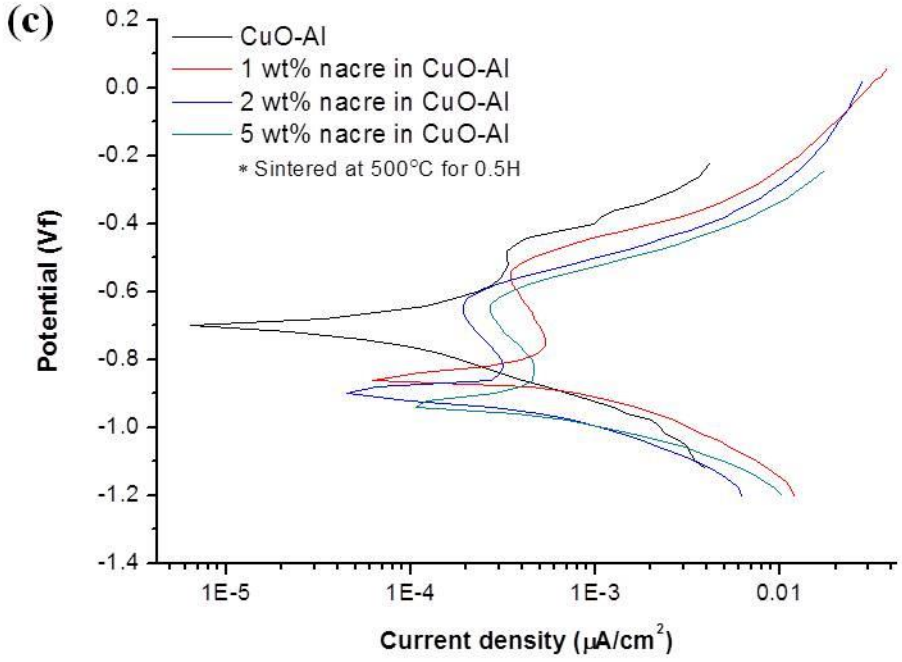

Figure 20 Continued.

Table 5. Corrosion rates of each specimen.

Composite	Nacre wt%	I_{corr}	E_{corr}	Corrosion rate
Nacre-Al	0%	5.230 μA	-1.130 V	17.66 mpy
	1%	1.570 μA	-1.020 V	5.311 mpy
	2%	2.400 μA	-1.010 V	8.120 mpy
	5%	4.380 μA	-918 mV	14.79 mpy
Nacre-Al-CuO (440℃, 6H)	0%	19.40 μA	-805 mV	65.27 mpy
	1%	2.260 nA	-721 mV	$7.613e^{-3}$ mpy
	2%	62.60 nA	-669 mV	$210.7e^{-3}$ mpy
	5%	151.0 nA	-755 mV	$509.5e^{-3}$ mpy
Nacre-Al-CuO (500℃, 0.5H)	0%	54.10 μA	-704 mV	181.9 mpy
	1%	662.0 μA	-853 mV	$2.227e^{3}$ mpy
	2%	474.0 μA	-904 mV	$1.596e^{3}$ mpy
	5%	929.0 μA	-930 mV	$3.127e^{3}$ mpy

4.3. Corrosion surface analysis

Corroded surfaces of each specimen were investigated under SEM and optical microscope. SEM and optical microscope revealed that specimens are underwent the intergranular and the galvanic corrosion. The localized corrosion along the grain boundaries is known as the intergranular corrosion. The galvanic corrosion occurs when two metals are contacted in an electrolyte. The noble metal corrodes preferentially to another metal [29].

Figure 21.(a) shows localized corrosion on the 1wt% nacre in CuO-Al composite surface. The intergranular corrosion attacks are identified along the grains boundaries and pulled out grain regions are observed

The corrosion occurred around specific grains on the specimens containing CuO in Figure 21.(b, c). This indicates corrosion is initiated and spread out from the phase II in Figure 21.(b). After sintering, CuO changed the color from black to orange like in Figure 21.(c). The reduction process may takes place on CuO grains and become Cu grains during the sintering. Because of the potential difference between Al and Cu, the galvanic corrosion takes place on the interface of Cu and Al grains.

In Figure 21.(d), there are relatively clean surface around nacreous particles and the impaired area (red arrow) is observed on nacreous particle. This indicates that nacreous particles are attacked during corrosion process.

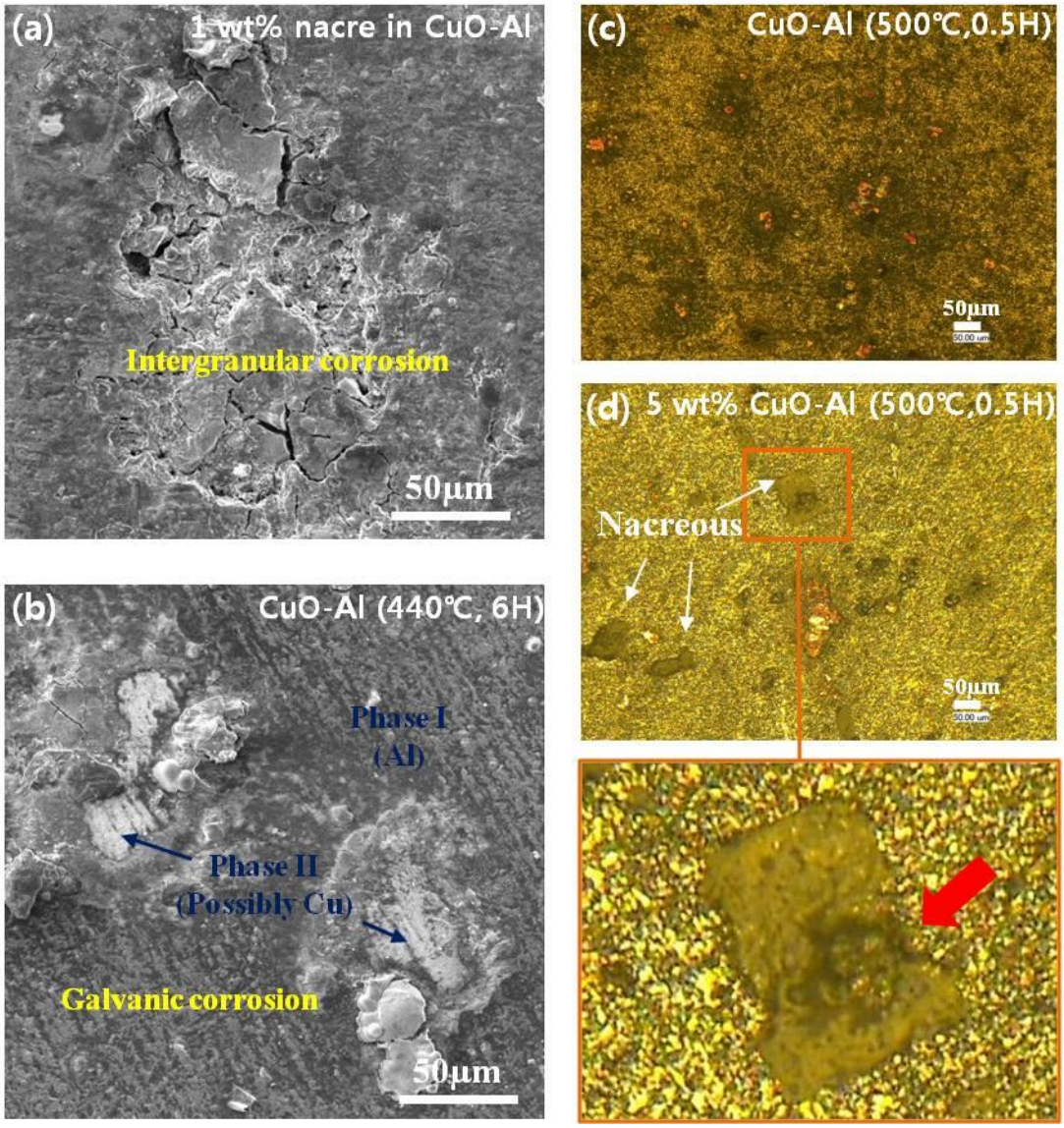

Figure 21. Observed intergranular and galvanic corrosion.

4.4. Mechanisms

Grain boundaries are crystallographic disordered atomic region [28]. Inherently, grain boundaries are imperfect and have a high energy structure. When grain boundaries are exposed to an electrolyte, the less noble grain boundaries have lower corrosion resistance [43].

In 1940, Dix reported the intergranular corrosion of Cu-Al alloys [44]. During heat treatment, Cu diffuses along grain boundaries. At the low quenching rate, the Al_2Cu are formed and precipitates at grain boundaries. The zone close to the grain boundaries become Cu-depleted zone [45]. Galvele and De Micheli reported Cl^- ions affect the intergranular corrosion of Cu-Al alloys. They studied the intergranular corrosion is caused by a difference of breakdown potential [46].

The specimens containing Cu show the intergranular corrosion. This mechanism was similar to Galvele and De Micheli reported. There are 3 phases to be explained a mechanism of the intergranular corrosion. The phase I is Cu-depleted zone. The Al grain bodies are phase II and the intermetallic precipitations are phase III (Figure 22). Each phase have different potentials. The potentials of each phase in Cu-Al alloys had reported. The potentials of the Cu-depleted zone, the Al grain bodies and the Al_2Cu precipitations are -750 mV, -690 mV and -640 mV respectively [45]. In the studied specimens, Al_xCu_y or $Al_xCu_yCa_z$ might be precipitated along the grain boundaries during sintering. The Cu-depleted zone could be formed in the vicinity of the grain boundaries. The Cu-depleted zone has higher breakdown potentials than the other phases. The Cl^-

ions will attack the Cu-depleted zone preferentially due to the potential differences and the grain boundaries are dissolved.

The reason why the corrosion initiated on the boundary of the Cu grains can be explained based on the galvanic corrosion. According to the electrode potential chart, the Al is less noble than the Cu. When the Al grains and Cu grains are contacted, the Al grains become an anode. The Cl^- ions take the electrons from the Al preferentially.

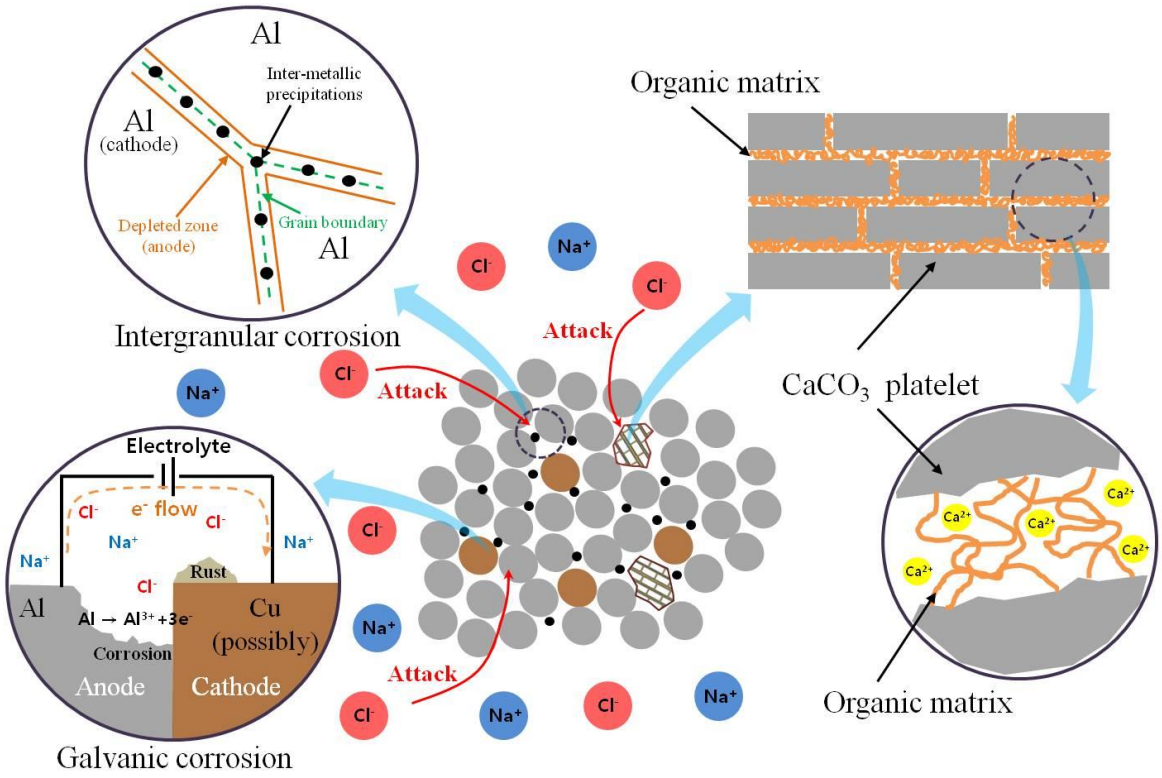

Figure 22. Corrosion mechanisms in nacre-reinforced composites.

The additions of nacreous result in a higher corrosion resistance of the composites. As discussed in Chapter I, 95% of the nacreous is $CaCO_3$ and rest of them are an organic matrix which are the mixture of proteins, chitin, polysaccharides, glycoproteins, carbonate and calcium. The Cl^- ions will preferably attack the Ca in the nacreous because the Ca is much active element than Al and Cu. This could be a possible mechanism the nacreous protect the Al from the corrosion attack.

CHAPTER V

TRIBOLOGICAL EVALUATION

This chapter discusses the effects of nacreous particles on wear. The contents start with discussion about hardness, one of the key properties dominating wear. Next, frictional behaviors are analyzed in order to check if nacreous influence on friction coefficient. Finally, the effects of nacreous on wear are discussed with wear evaluation and mechanisms.

5.1. Hardness

The procedure of hardness measurement was described in Chapter III. Results are discussed in the following.

5.1.1. Hardness

The hardness data is shown in Figure 23. Results show that in nacre-Al and nacre-CuO-Al composites, as nacreous concentration increases, hardness increases. Aluminum-copper oxide composite has higher hardness. Different sintering temperature and time affected the hardness. In nacre-Al and nacre-CuO-Al composites, 2 wt% nacreous concentration shows slightly higher hardness than that of 1 wt%. The sample having 5 wt% nacreous concentrations is clear to be harder than the reference. Especially, this specimen was sintered at 500°C for 0.5 hour with an increase of 32% in comparison with the pure aluminum. In the group of 7.9wt% CuO in Al specimens, longer sintering time reduce the hardness value. Longer heating time introduces the recrystallization of

the aluminum matrix. This is the reason why 7.9 wt% CuO in Al which sintered at 440°C for 6 hours show lower hardness value.

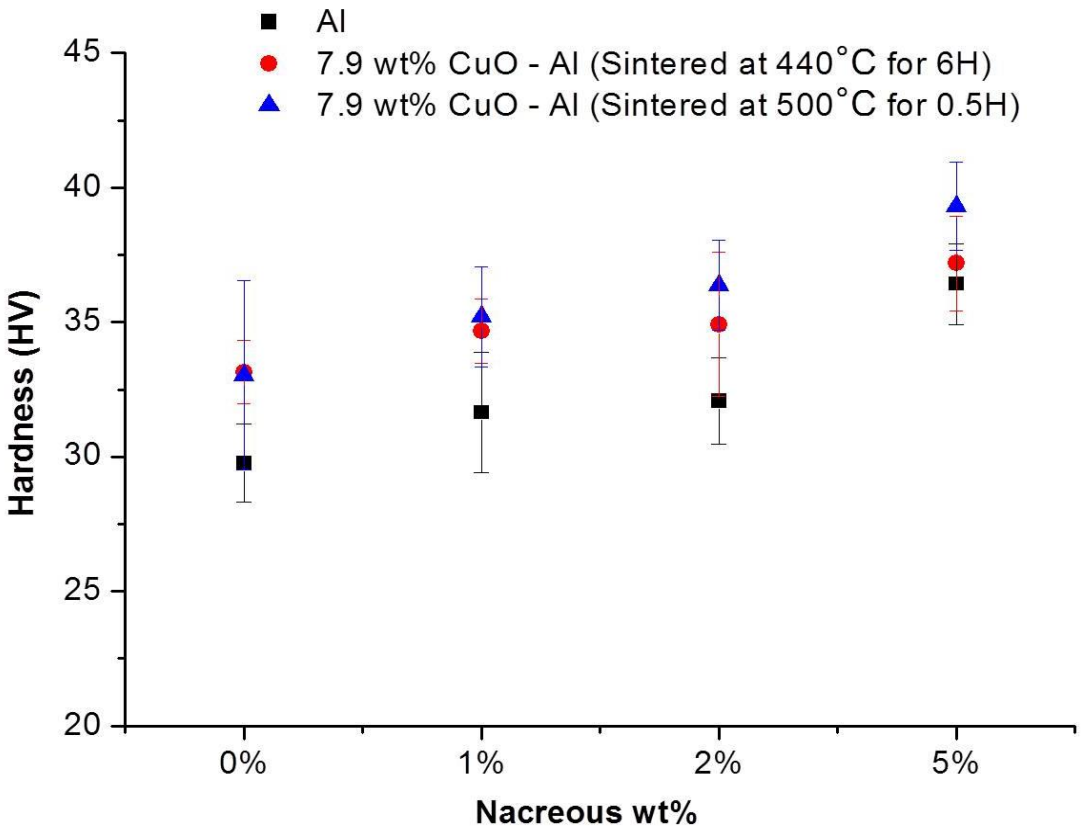

Figure 23. Vickers hardness test results.

5.1.2. Particle size and shape

Particle size and shape affect the hardness. The way of strengthening metals are restricting the dislocation motion. Hindering the mobility of dislocation influence on

how easy plastic deformation happens. Low dislocation mobility and high tendency of plastic deformation occurring enhance the hardness. One of strengthening mechanism is reducing the grain size. A small grained material has more grain boundaries to restrict dislocation motion. [31]. Figure 24 shows grain size and shape of powders.

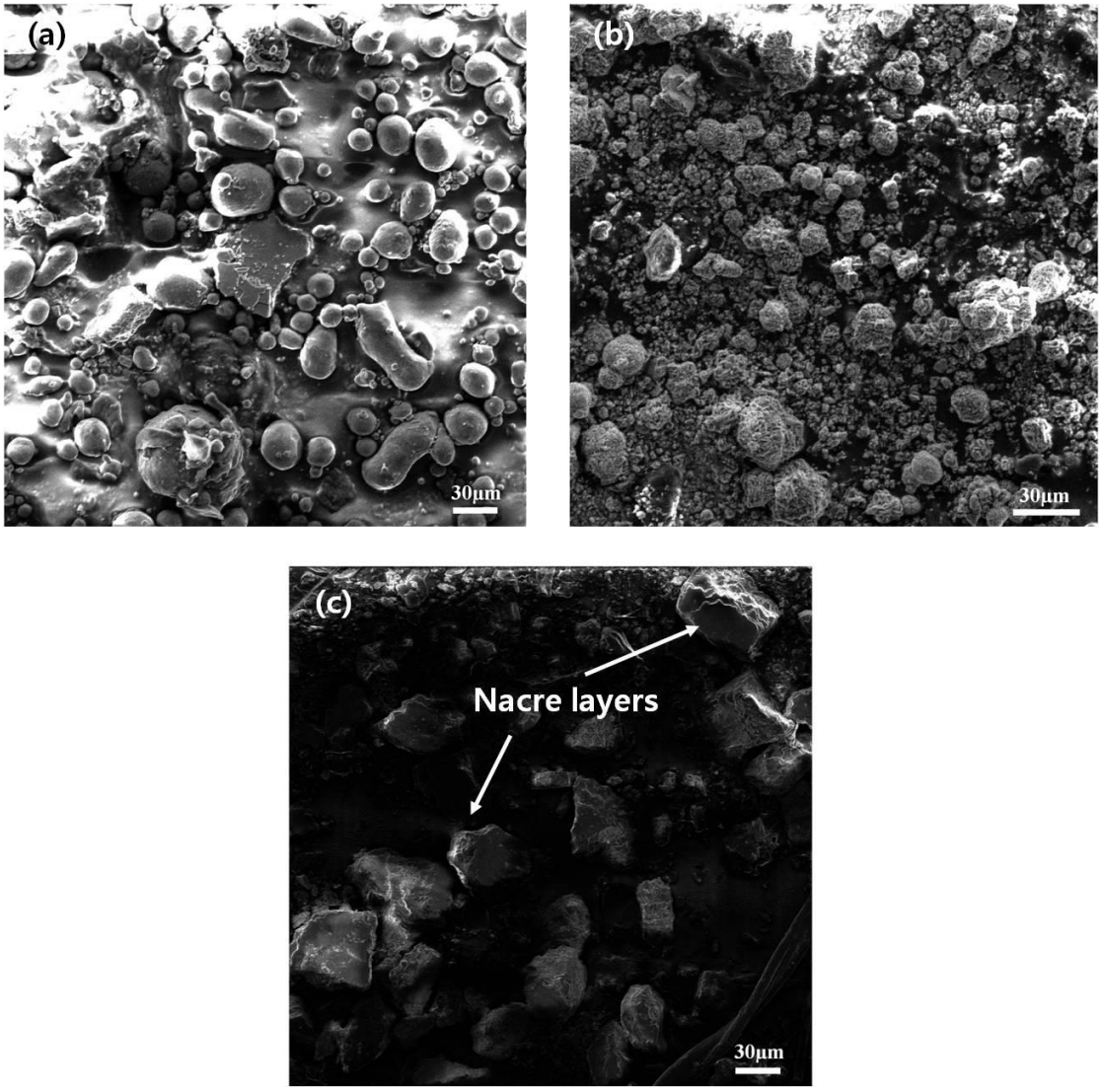

Figure 24. Grain size and shape of the used powders (a) Al (b) CuO (c) nacreous

The Al and CuO powder has about 5 μm ~ 30 μm grain size in spherical shape. The nacreous powder has more wide range of grain size from 5 μm ~ 53 μm in irregular polygonal shape. In Figure 24 (c), the arrows indicate nacreous layers in seashell powder.

5.1.3. Increased oxygen

The specimens containing CuO show higher hardness. The presence of the oxygen in CuO-Al composites could be a reason. EDS mapping analysis was conducted to evaluate the amount of the oxygen. Figure 25 shows the EDS mapping images before and after sintering of the CuO-Al composites.

EDS analysis indicated that more oxygen was observed after sintering. The amount of oxygen was increased up to twice as pre-sintering in the CuO-Al composite. Most likely because oxidation took place on the matrix and Al_2O_3 are formed. In Figure 26, CuO-Al composite has more amount of oxygen than pure Al. During the sintering, Al obtains more oxygen from either CuO or air. The increased amount of oxygen is the reason that the specimens containing CuO show higher hardness than Al based composites.

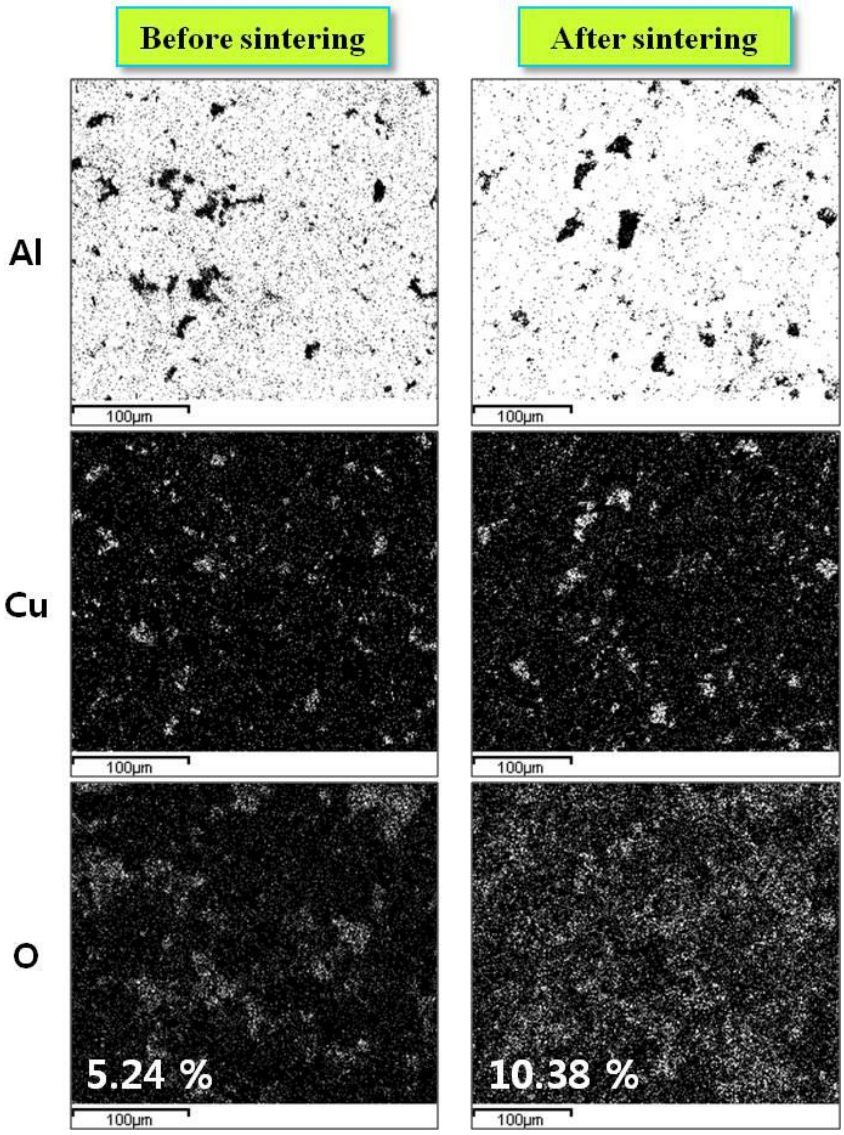

Figure 25. The energy-dispersive X-ray spectroscopy analysis.

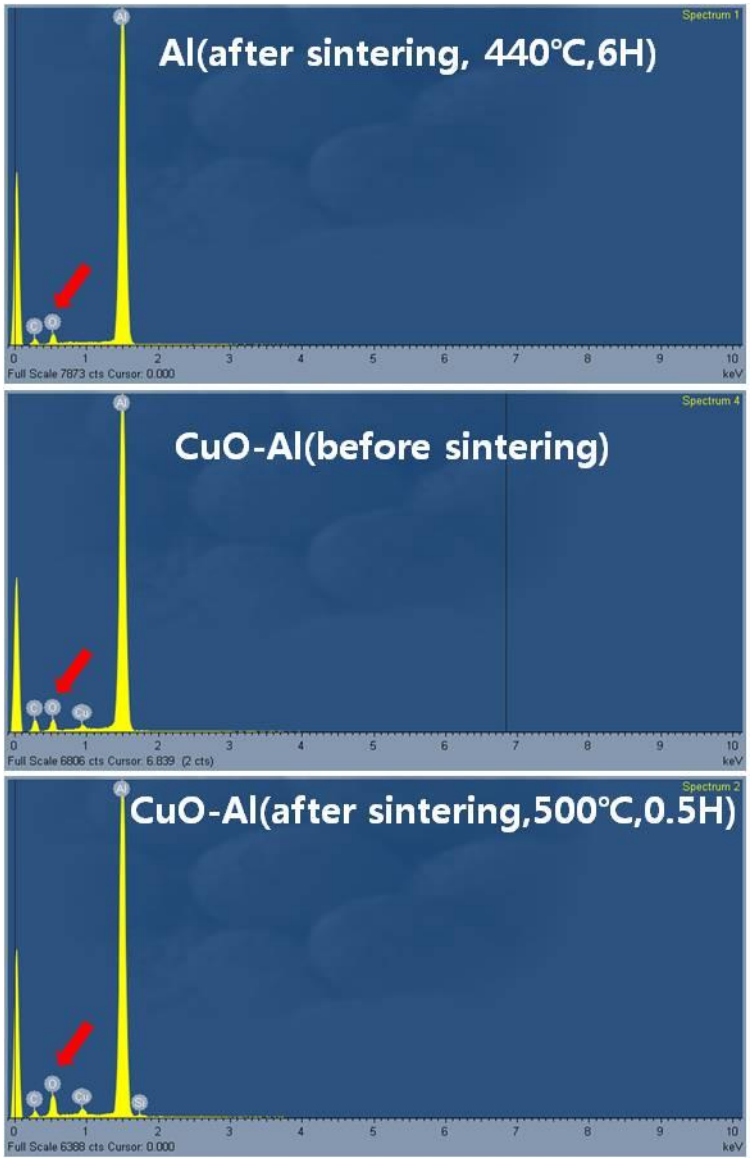

Figure 26. Increased oxygen in the composite.

5.1.4. Hardening mechanism

There are two types of particle-reinforced composites made here: large particle and dispersion strengthened composites. Reinforced particle size is the only difference between particle reinforced composites. Large-particle composites are considered as a

continuum mechanics. The particle-matrix interactions are not dealt with at the atomic or molecular level. When the reinforced particles size are 10 ~ 100 nm, it is treated on dispersion strengthened composites [31]. In this study, hardening mechanism follows the large particle reinforced composites.

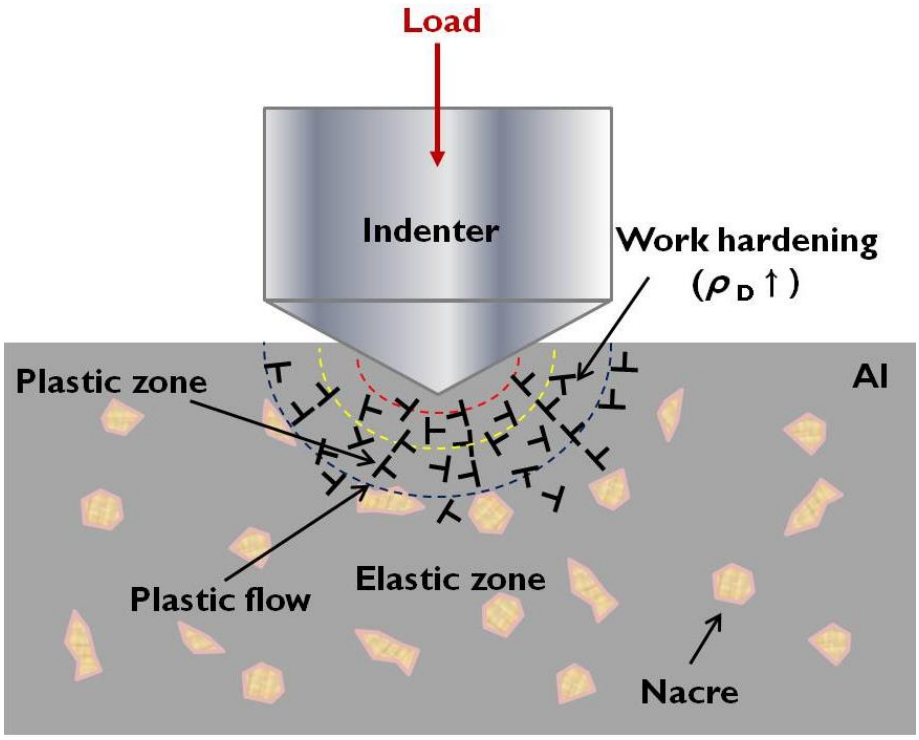

Figure 27. Hardening mechanism.

During the hardness test, impressing tip of indenter generates stress in the vicinity of indentation. As a consequence, dislocations are generated and local plastic deformation takes place along the plastic flow line. As the indenter moves down,

dislocation mobility increases and more dislocations are generated. When the dislocations meet the nacreous particles, the nacreous particles hinder the dislocation movement. The dislocations are not able to move further. Dislocation density in the plastic zone increases because of dislocations pile up and new dislocations form continuously. The distance between the each dislocation decreases and become close together. Closed dislocations hinder their movement and work hardening occurs. This is the reason that why the higher concentration of nacreous particles increase hardness. This process is schematically illustrated in Figure 27.

5.2. Frictional behavior

Results in Figure 28 showed that the friction of all samples was about the same. In the figure, Al and 1 wt% Al shows relatively higher friction coefficient but most case of each specimen represent similar mean values and overlapped error bars. In the friction coefficient versus time graphs (Figure), all cases show very similar movements of plot. This indicates that nacreous does not influence on friction coefficient. This is because non-abrasive nacreous particles don’t increase the friction coefficient and friction coefficient test was conducted without any lubrication.

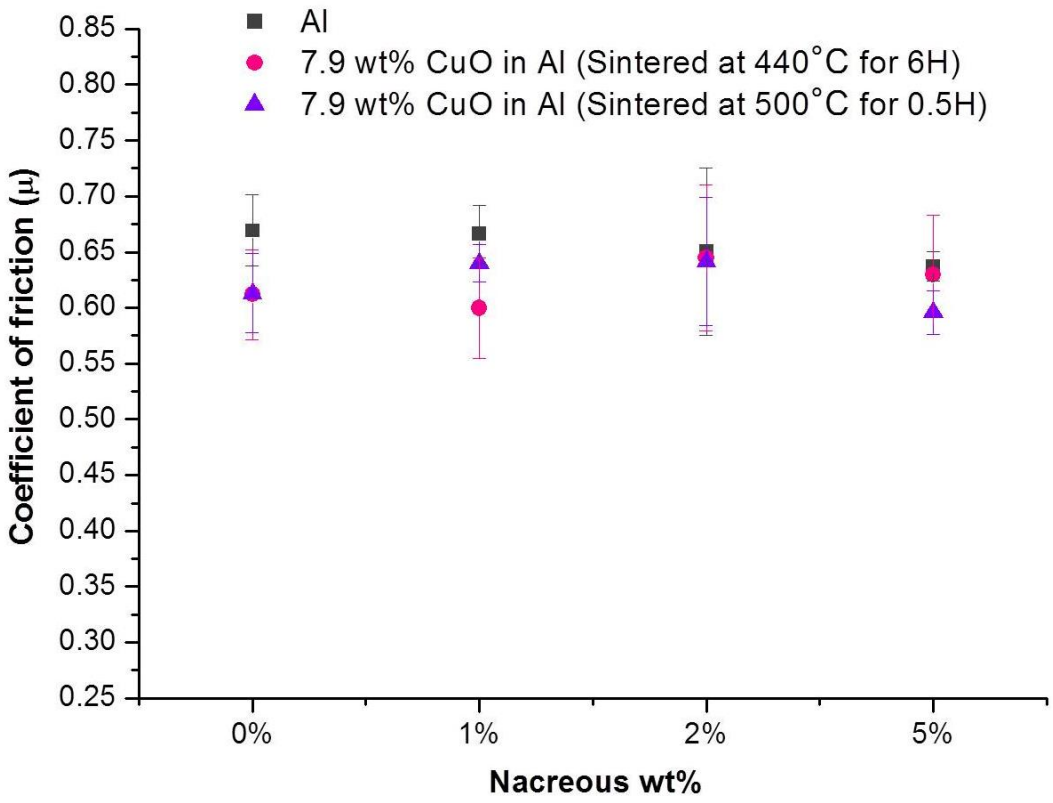

Figure 28. Friction coefficient test results.

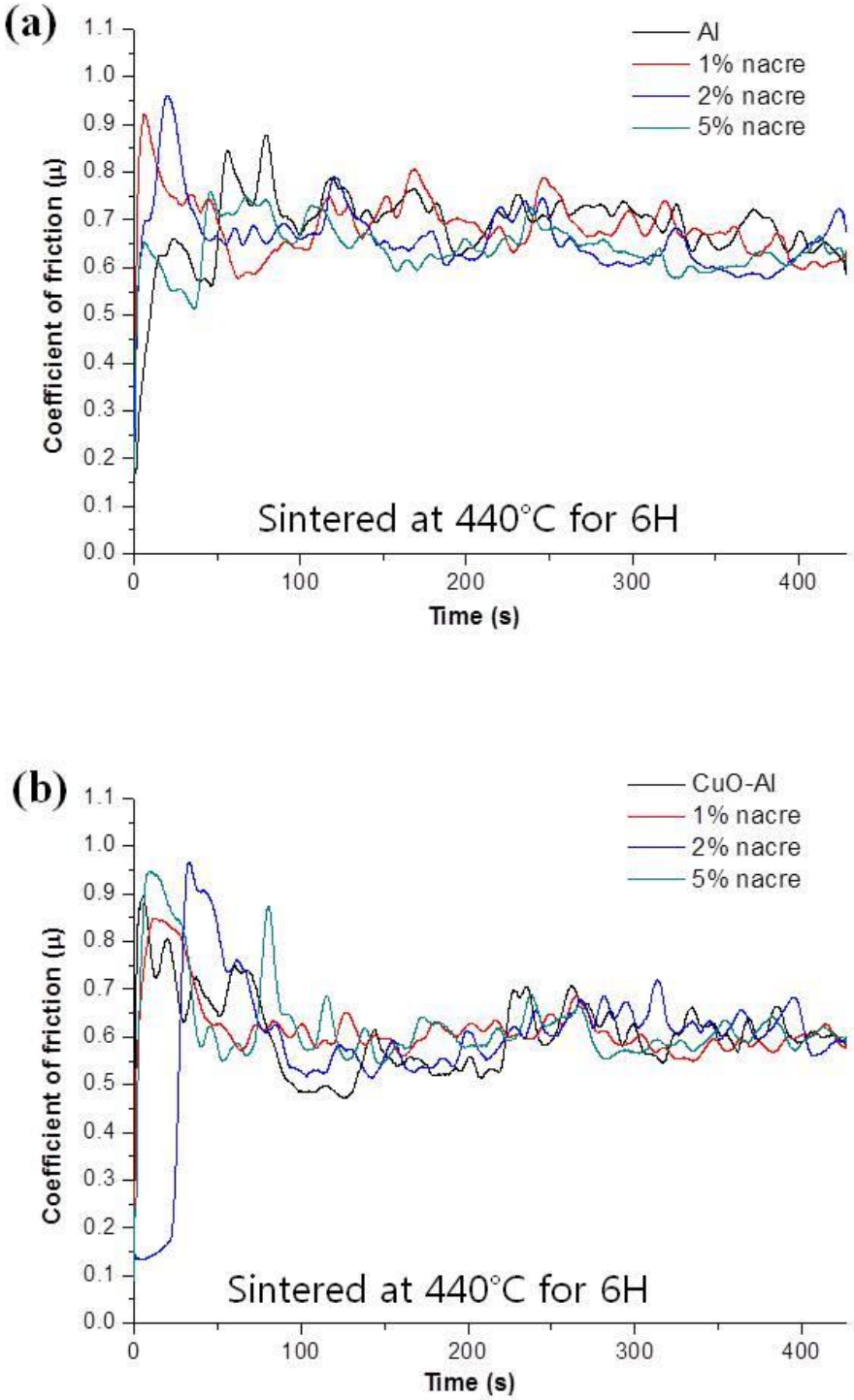

Figure 29. Friction coefficient versus time plots.

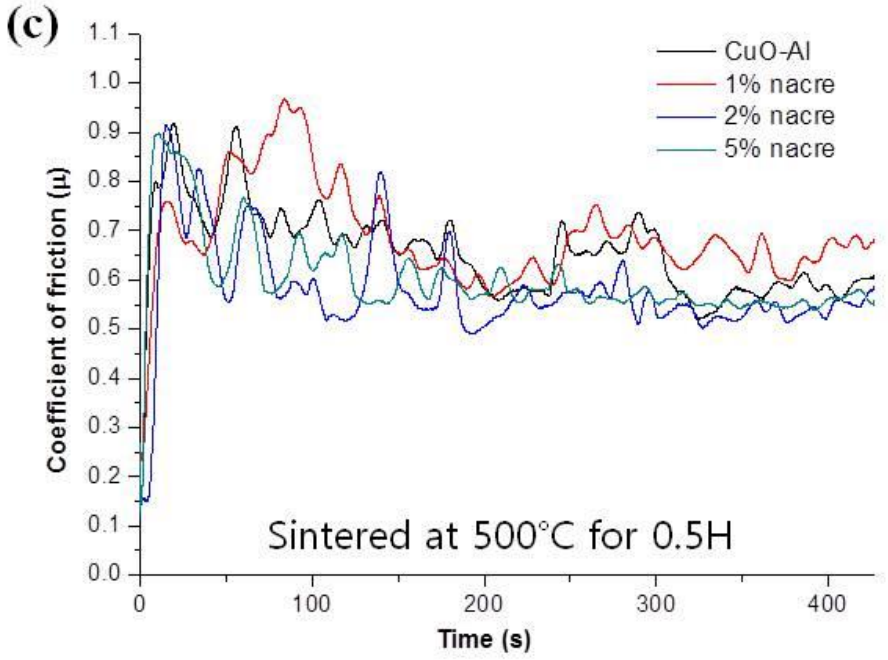

Figure 29 Continued.

5.3. Wear study

Wear test results are discusses in the following sections. The effects of nacreous on wear are analyzed with SEM images.

5.3.1. Wear volume and rate

According to Archard equation, as the hardness increases wear resistance increases. The addition of nacreous increases the hardness of all reference specimens (Al and 7.9 wt% CuO-Al with different sintering time). In the wear volume loss versus nacreous concentration chart in figure 8, reference specimens lost more wear volume than the specimens with nacreous. However, there are no big differences on wear volume loss among 1, 2 and 5 wt % nacreous concentrations except 5 wt% nacre in

CuO-Al (sintered at 500°C for 0.5H). The 5 wt% nacre in CuO-Al (sintered at 500°C for 0.5H) decreases 37% wear volume loss compare to the pure aluminum.

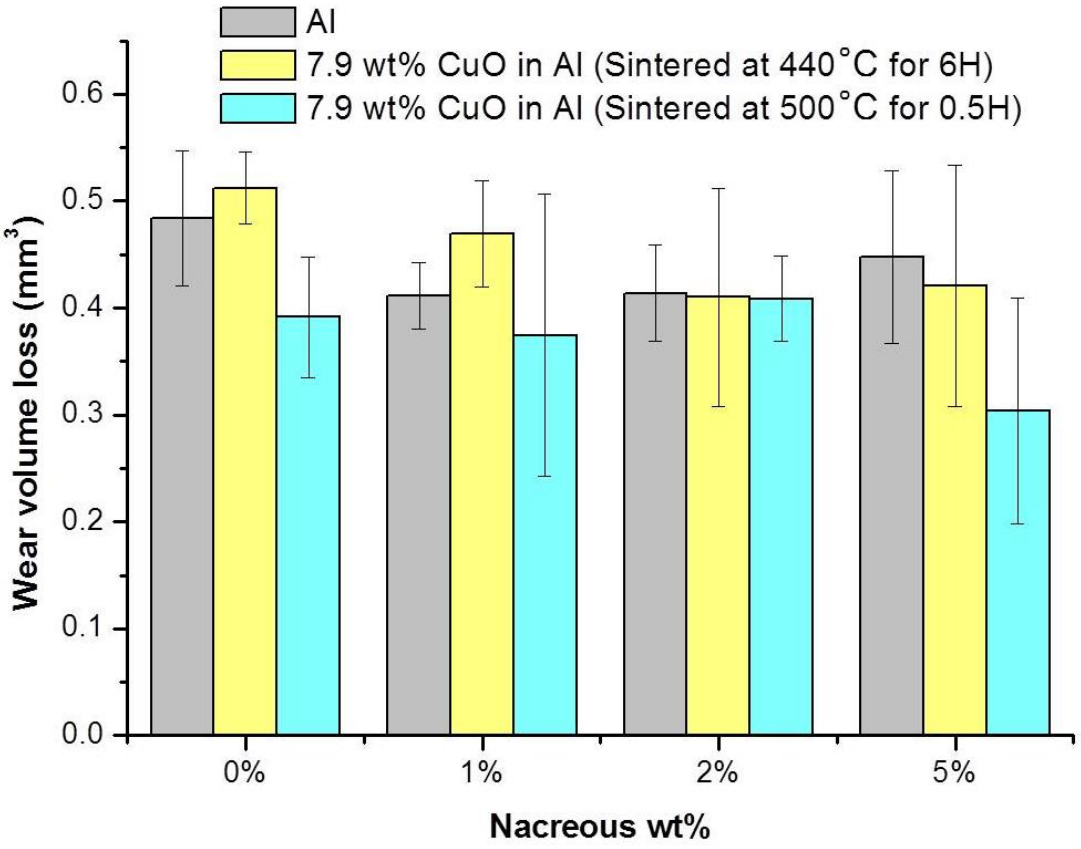

Figure 30. Wear test results.

5.3.2. Wear mode analysis

Worn surfaces of each specimen was analyzed using an SEM. Pure Al, 1 wt% nacre in Al, 2 wt% nacre in CuO-Al (sintered at 440C for 6 hours), and 5 wt % nacre in

CuO-Al (sintered at 500C for 0.5 hours) composite were analyzed based on the hardness and wear test results. Abrasive and adhesive wear mechanisms were observed in general under dry sliding condition.

On pure Al wear surface, observed wide and deep grooves are the evidence of the abrasive wear mechanism (Figure 32.a). When the hard curved surface of the counter face (stainless steel ball) contacts the relatively soft surface of the Al, two surfaces are interlocked. Hard counter face ploughs the soft surface of the Al. As a result, Al undergoes volume loss and grooves are formed on the surface. Forming a groove indicates that the material is ductile. The groves formed due to abrasive wear [34].

Brittle fracture was also observed on the Al surface. In case of abrasive wear on brittle material, ploughing cause a median or lateral crack [34]. The top arrow in the Figure 33.(a) indicates lateral crack on the Al. The abrasive wear mode of brittle and ductile material are illustrated in Figure 31.(a).

The adhesive wear was present in and near the grooves in Al. This was evidenced with large pull-outs found on the wear surface as shown in the Figure 10, more so on the wear track. In the same figure, Figure 32.(e, f), there were wear particles found on the stainless steel ball. This process is illustrated in Figure 31.(b).

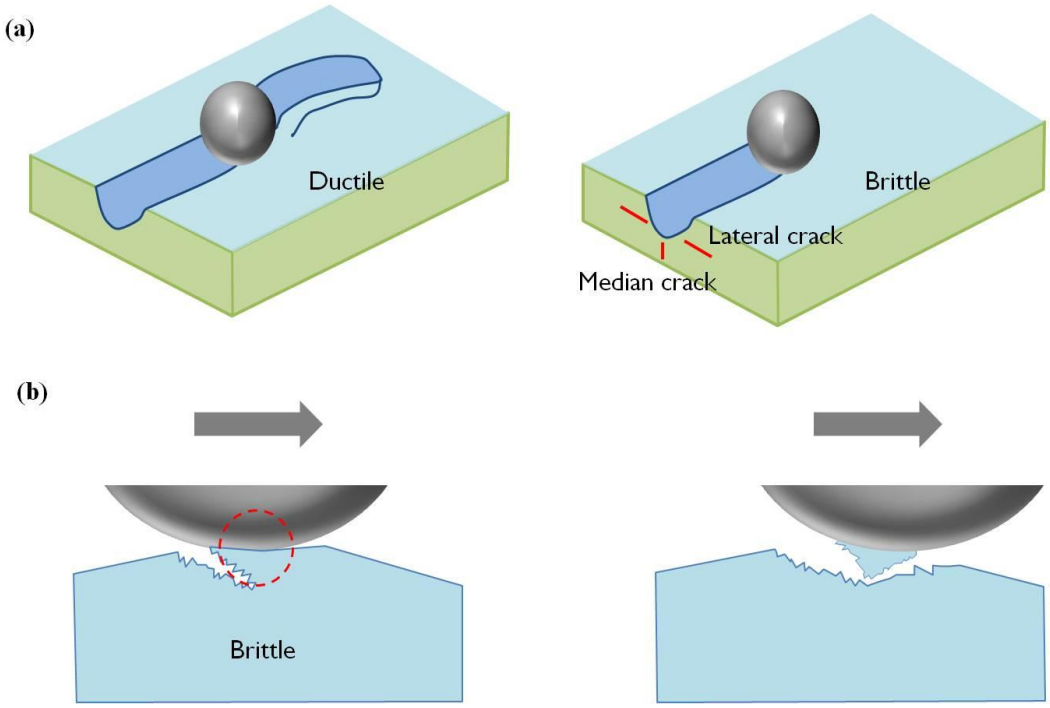

Figure 31. Wear mode (a) abrasive (b) adhesive.

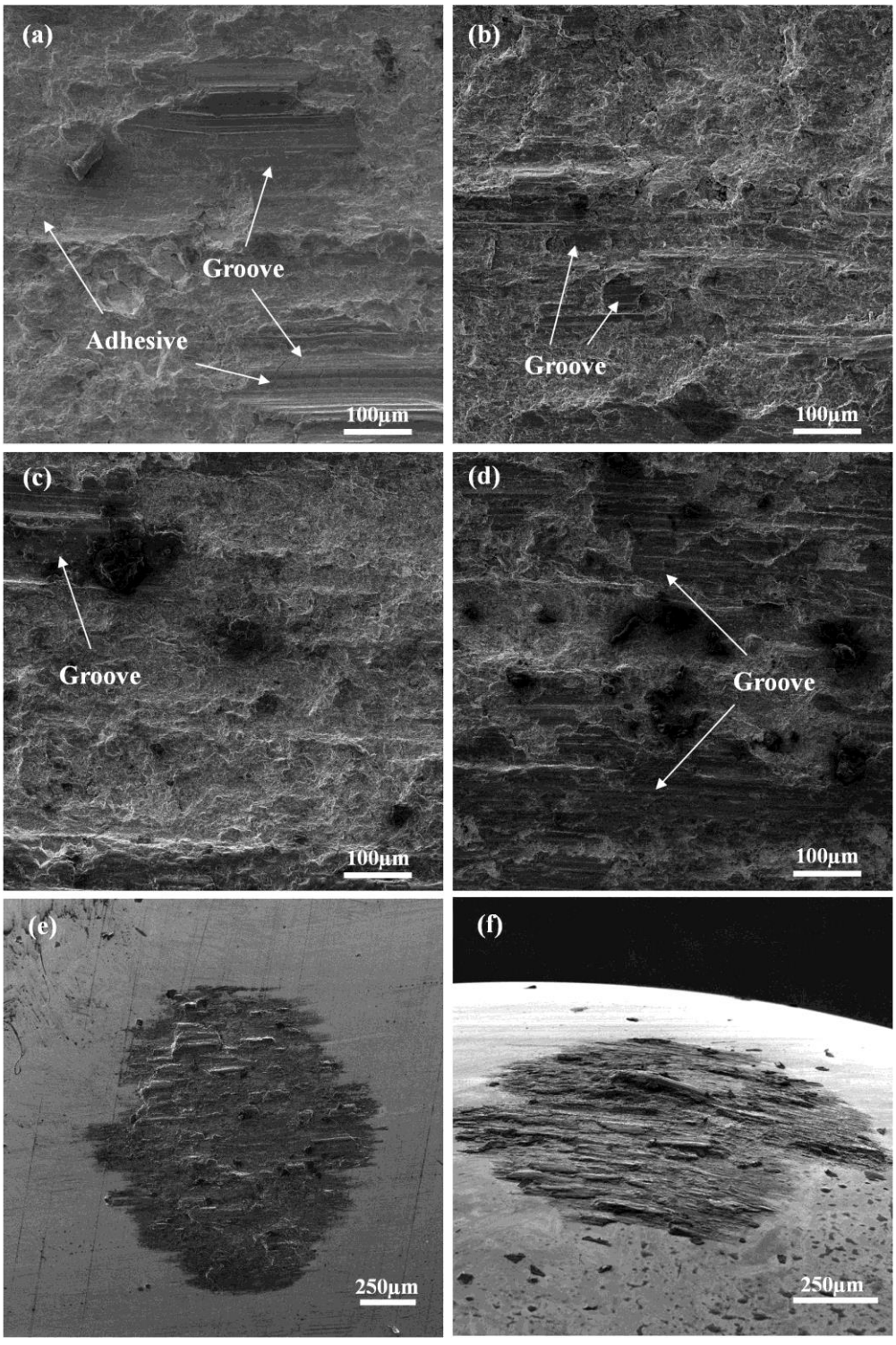

Figure 32. Worn surfaces

Samples of 1 wt% nacre-Al and 2 wt% nacre-CuO-Al (sintered at 440C for 6 hours) show the brittle characteristic. These composites have abrasive and adhesive wear mechanism like pure Al, but Figure 32. (b, c) shows less grooves and larger fractured wear surface than pure Al. This phenomenon demonstrates that the material became more brittle.

On the surface of the 5 wt% nacre-CuO-Al (sintered at 500C for 0.5 hours) composites, an evidence of the material recovered the ductility was identified. As seen in Figure 32. (d), wide fractured areas exist on the wear track but wide grooves are observed like pure Al. This mechanism is followed by the characteristic of nacreous microstructure. The unique brick and mortar type nacreous architecture enhances the fracture toughness.

For further investigation of wear mechanisms, cross section of the wear tracks are observed. On the cross section of pure aluminum, deep and long grooves are observed parallel to sliding direction (Figure 33.a). Lateral crack is observed as well. A sample of 1 wt% nacre-Al composite shows fewer grooves and more fractured surface. This indicates that 1 wt% nacre-Al composite has more brittleness than Al. The grooves exhibit again in 5 wt% nacre-CuO-Al composite (sintered at 500°C for 0.5 hours). The morphological characteristic represents that the mechanical behaviors are changed between ductile and brittle.

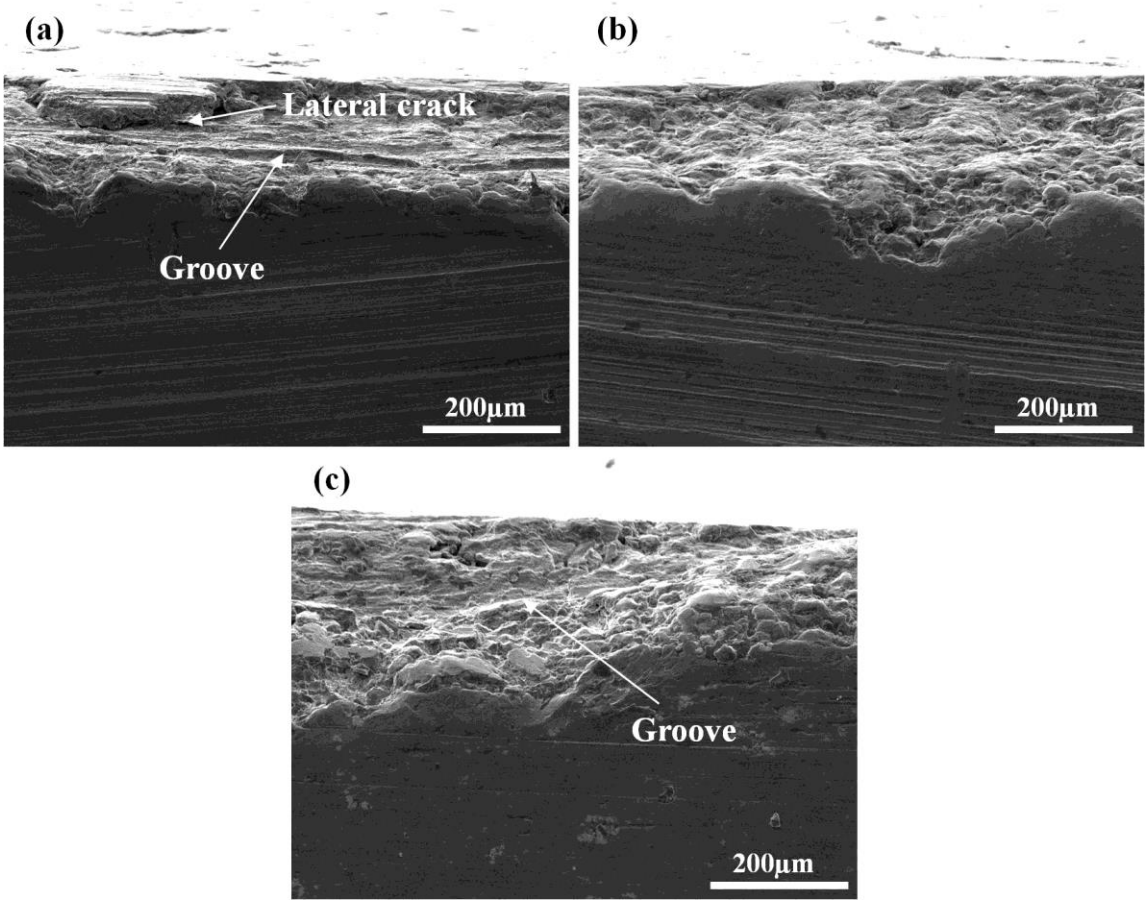

Figure 33. Cross sections of wear tracks.

Wear debris were collected after wear test in order to study wear mechanisms. The size of wear debris depends on the wear resistance of the material. Comparing the wear particle size provides the information of wear mechanism.

Samples of 1 wt% nacre in Al, 2 wt% nacre-CuO-Al (sintered at 440°C for 6 hours) and 5 wt% nacre-CuO-Al composite (sintered at 500°C for 0.5 hour) mostly consist of small wear particles whereas pure Al has relatively large wear particles ().These debris are brittle in nature and might be formed due to crack propagation. If the material has a poor

crack resistance, cracks propagate further. The counter-face push the propagated surface and wear particles are pulled out from the surface. As a result, large wear particles are formed.

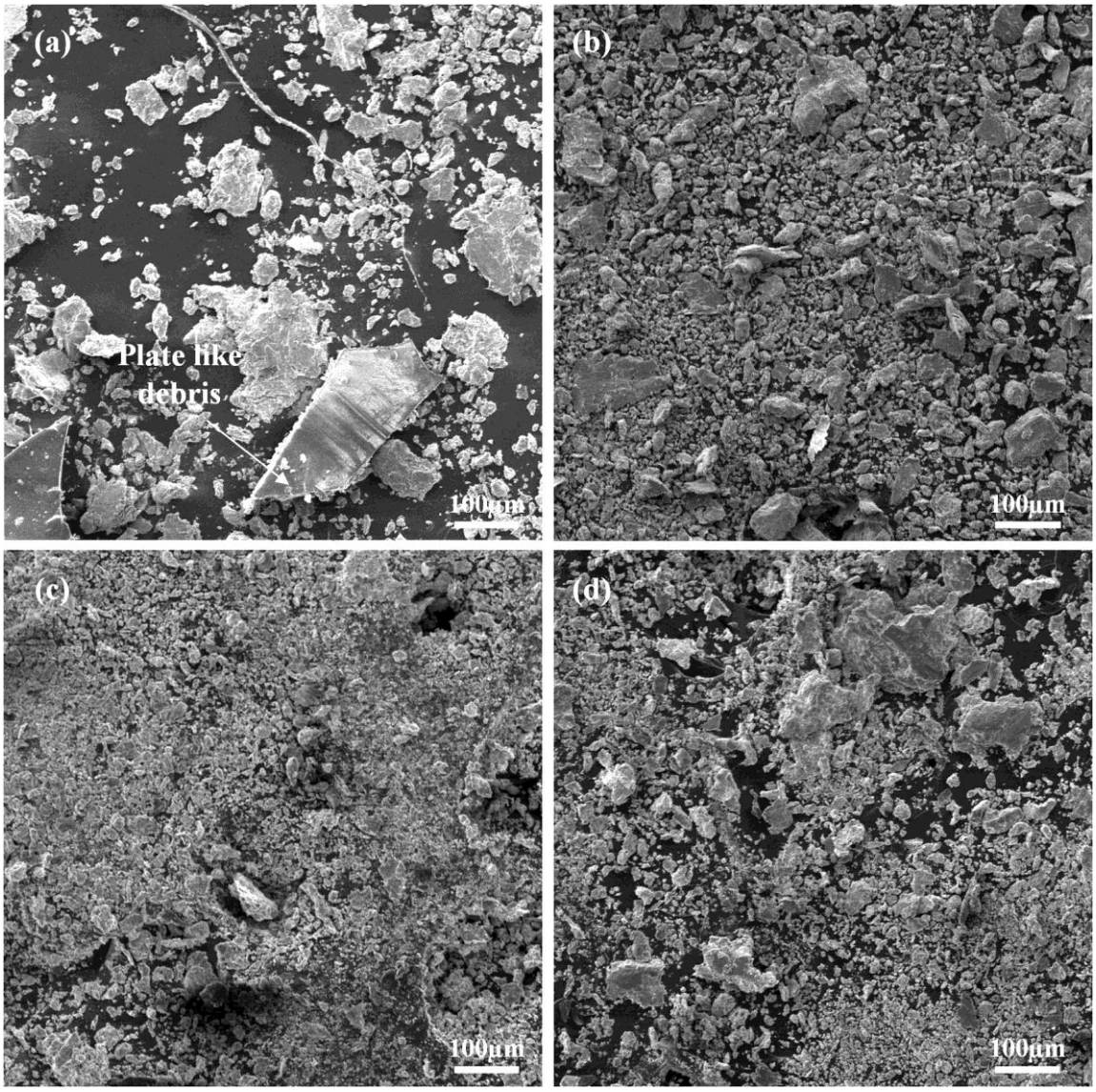

Figure 34. Wear debris.

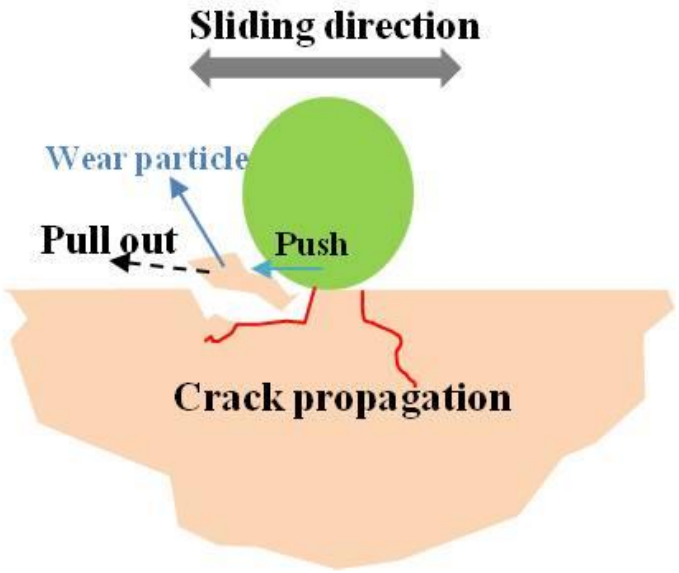

Figure 35. The process of generating large wear particles.

5.3.3. Mechanisms

A crack propagated toward the nacreous particles and was blocked by nacreous particle (Figure 36). The generated cracks' paths were linked to nacreous particles. The nacreous has the irregular polygonal shape and poor interfacial bonding between matrix and nacreous. The voids are formed around nacreous and cracks propagate toward nacreous particle.

As mentioned in Chapter I, the nacreous layers are interlocked with the wavy shaped platelets and nanoasperities on the surface. These nanostructural features provide crack resistance in the composites (Figure 37.a).

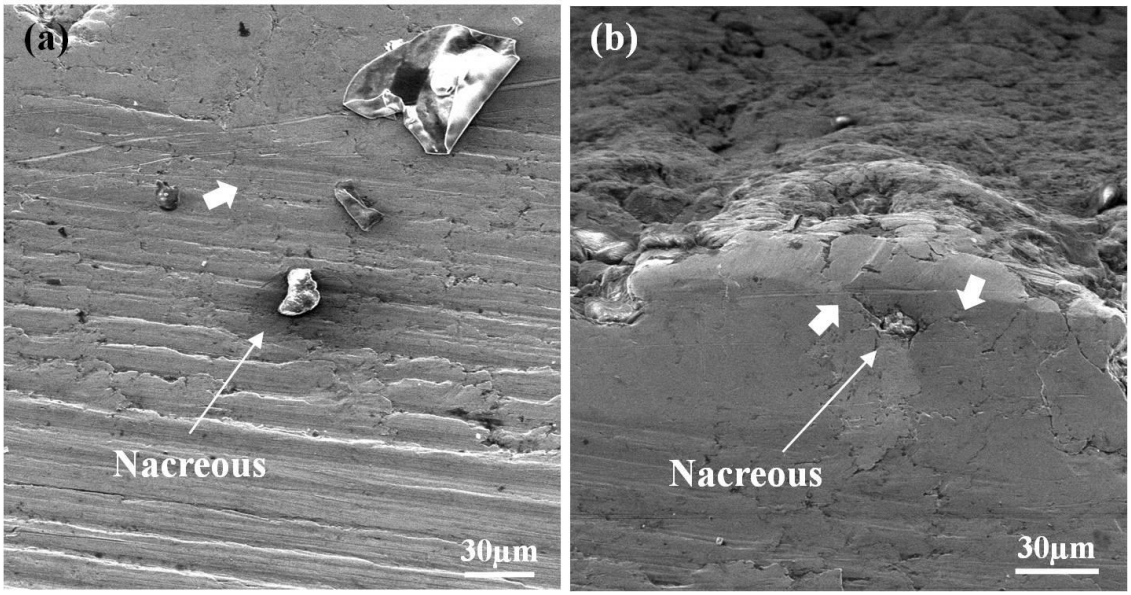

Figure 36. Nacreous particle blocks crack propagation.

When the crack propagates to nacreous particle in the composite, nacreous layers are exposed to tensile strength. Until a critical loading point before fracture, layers begin to slide within a dilatation band. The slip of the platelet in the dilatation band is restrained due to the nanoasperities on the platelet surface. To pass the asperities for further sliding, the material dilates to transversal direction. This dilatation causes the compressive stress in the dilatation band which contributes the strain hardening [14]. Higher resistance of shear stress is required to achieve strain hardening. The nanoasperities and waviness of the aragonite platelets increase friction between two adjacent rows of platelet. [8, 14].

The brick and mortar type architecture of the nacreous is another main source of crack resistance (Figure 37.b). The aragonite platelets are hard and brittle. The interfaces

between the aragonite plates are relatively soft. When the crack propagates and encounters the nacreous particle in the composite, the crack deflection takes place along the interfaces between the aragonite plates. These two mechanisms increase wear resistance.

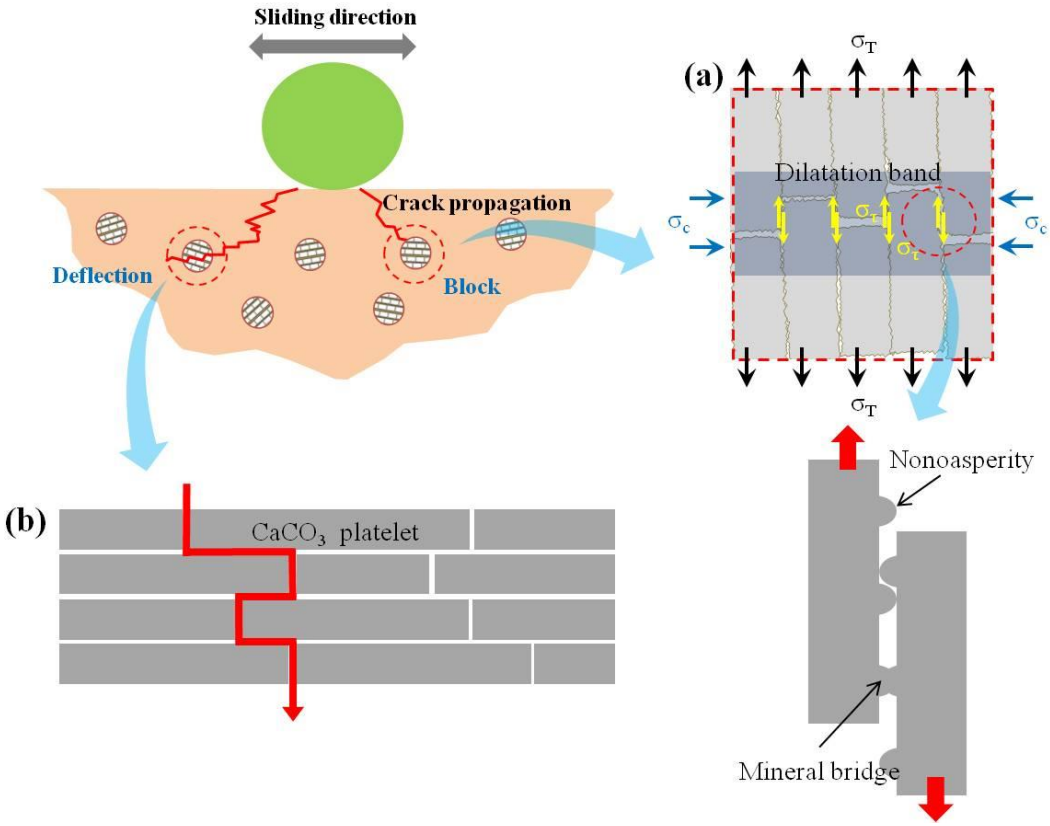

Figure 37. Crack resistance of nacreous in composite.

CHAPTER VI

CONCLUSIONS AND FUTURE RECOMMENDATIONS

6.1. Conclusions

A novel composite has been developed to improve corrosion and wear resistance. The nacreous-reinforced-aluminum matrix composite is produced using a powder metallurgy process. Evaluation of properties and behavior of the material was carried out using various experimental techniques, including electrochemical, indentation, and tribological tests. Followings are the main findings in this research.

1. Nacreous particles increase corrosion resistance. The calcium in the nacreous particles protects the matrix from corrosion attack.
2. As the nacreous concentration increases, the hardness increases. The interlocked nacreous microstructure enhances the hardness. During the hardness test, nacreous particles block the motion of dislocations, and the dislocation density increases. Work hardening takes place due to closed dislocations and hardness increases.
3. The specimens containing CuO show higher hardness. EDS mapping analysis revealed that oxidation takes place on the matrix during the sintering. A sample of 5 wt% nacre in CuO-Al (sintered at 500°C for 0.5h) shows 32% higher hardness than the reference specimen of pure Al.

4. Nacreous increases wear resistance. The structure of nacreous enables blocking of crack propagation. As such the 5wt% nacre in CuO-Al (sintered at 500°C for 0.5h) decreases 37% wear volume loss compared to pure Al.

6.2. Future recommendations

In the case of the nacreous particle, the thickness of the nacreous layers is one of the key factors for enhancement. Thick nacreous layers enhance their hardness and fracture toughness. There will be critical nacreous particle size to obtain the best hardness as the reinforcement. The critical nacreous particle size should be determined.

Experimental validation of the proposed corrosion mechanism is suggested to be carried out.

REFERENCES

[1] H. Yahya, "Biomimetics: Technology imitates nature", *Global Publishing*, Okmeydani-Istanbul, Turkey, pp103-123, 2006.

[2] A. G. Melvin, "Color treasury of seashells", *Crescent Books*, London, United Kingdom, pp12-42, 1973.

[3] M. G. Harasewych and F. Moretzsohn, "The shells" In The book of shells, edited by M. G. Harasewych, The *University of Chicago Press,* Chicago*,* pp26-637, 2010.

[4] L. Brix, "New record: world's oldest animal is 507 years old", Science Nordic, [Cited 04/20/2014]; Available from: http://sciencenordic.com/new-record-world%25E2%2580%2599s-oldest-animal-507-years-old.

[5] K. Y. Johnstone, R. Freund and R. Martin, "Sea treasure: A guide to shell collecting", *Houghton Mifflin Hardcourt Publishing Company,* Cambridge, pp13-23, 1957.

[6] J. M. Eisenberg, "A collector's guide to seashells of the world", *McGraw-Hill Book Company*, New York, pp24-32, 1981.

[7] F. Marin and G. Luquet, "Molluscan shell proteins", *C. R. Palevol*, **3**(6-7), France, pp469-492, 2004.

[8] C. Salinas and D. Kisailus, "Fracture mitigation strategies in gastropod shells", *JOM*, **65**(4), pp473-480, 2013.

[9] K. Akella, "Biomimetic designs inspired by seashells", *Resonance*, **17**(6), pp573-591, 2012.

[10] B. Ji and H. Gao, "A study of fracture mechanism in biological nano-composites via the virtual internal bond model", *Materials Science and Engineering A*, **366**(1), pp96-103, 2004.

[11] T. Furuhashi, C. Schwarzinger, I. Miksik, M. Smrz and A. Beran, "Molluscan shell evolution with review of shell calcification hypothesis", *Comparative Biochemistry and Physiology, Part B*, **154**(3), pp351-371, 2009.

[12] M. A. Meyers, A. Y. Lin, P. Chen and J. Muyco, "Mechanical strength of abalone nacre: Role of the soft organic layer", *Journal of the Mechanical Behavior of Biomedical Materials*, **1**(1), pp76-85, 2008.

[13] L. Genio, S. Kiel, M. R. Cunha, J. Grahame, C. T.S. Little, "Shell microstructures of mussels (Bivalvia: Mytilidae: Bathymodiolinae) from deep-sea chemosynthetic sites: Do they have a phylogenetic significance?". *Deep-sea Research I,* **64**(1), pp86-103, 2012.

[14] R. Wang, H. S. Gupta, "Deformation and fracture mechanisms of bone and nacre", *Annu. Rev. Mater. Res*., **41**(41-73), pp41-73, 2011.

[15] R.Z. Wang, Z. Suo, A.G. Evans, N. Yao, I.A. Aksay, "Deformation mechanisms in nacre", *J. Master. Res*., **16**(9), pp2485-2493, 2001.

[16] I. Corni, T.J. Harvey, J.A. Wharton, K.R. Stokes, F.C. Walsh and R. J. K. Wood, "A review of experimental techniques to produce a nacre-like structure", *Bioinspiration & Biomimetics.,***7**(3), 031001, 2012.

[17] M. Singla, D. D. Dwivedi, L. Singh and V. Chawla, "Development of aluminum based silicon carbide particulate metal matrix composite", *Journal of Minerals & Materials Characterization & Engineering*, **8**(6), pp.455-467, 2009.

[18] C. Cayron, "Aluminum matrix composites: processing and properties", Laussane, EPFL, [Cited 03/26/2014]; Available from: http://cimewww.epfl.ch/people/cayron/Fichiers/thesebook-chap2.pdf

[19] A. W. Fligier, L.A. Dobrzanski, M. Kremzer and M. Adamiak, "Manufacturing of aluminum matrix composite materials reinforced by Al_2O_3 particle", *Journal of Achievement in Materials and Manufacturing Engineering*, **27**(1), pp99-102, 2008.

[20] M. Lieblich, J. Corrochano, J. Ibanez, V. Vadillo, J. C. Walker and W. M. Rainforth, "Subsurface modifications in powder metallurgy aluminum alloy composites reinforced with intermetallic $MoSi_2$ particles under dry sliding wear", *Wear*, **309**(1-2), pp126-133, 2014.

[21] J. C. Walker, W. M. Rainforth and H. Jones, "Lubricated sliding wear behavior of aluminum alloy composites", *Wear*, **259**(1-6), pp577-589, 2005.

[22] A. M. Al-Qutub, A. Khalil, N. Saheb and A. S. Hakeem, "Wear and friction behavior of Al6061 Alloy reinforced with carbon nanotubes", *Wear*, **297**(1-2), pp752-761, 2013.

[23] A. R. Thryft, "Aluminum composite to lower weight in brake rotor", DesignNews, [Cited 04/20/2014]; Available from: http://www.designnews.com/author.asp?doc_id=239090&page_number=2&dfpPParams=ind_183,industry_auto,industry_gov,bid_27,aid_239090&dfpLayout=blog

[24] REL, "Metal matrix composite", REL. Inc, [Cited 04/20/2014]; Available from: http://www.relinc.net/adv-materials/metal-matrix-composite/

[25] B. Torres, M. Lieblich, J. Ibanez and A. Garcia-Escorial, "Mechanical properties of some PM aluminide and silicide reinforced 2124 aluminum matrix composites", *Scripta Materialia*, **47**(1), pp45-49, 2012

[26] BOSCH, "Brake systems", Bosch automotive technology, [Cited 04/20/2014]; Available from: http://www.bosch-automotivetechnology.com/en/de/driving_safety/driving_safety_systems_for_commercial_vehicles/bremssysteme/bremssysteme_1.html

[27] Winnetka shell, “New hope brake service”, Winnetka shell auto service, [Cited 04/20/2014]; Available from: http://www.winnetkashell.com/auto-repair/brake-service/

[28] L. M. Bacon, “3 vehicles contend to replace Marines’ Humvees”, Marine corps times [Cited 04/20/2014]; Available from: http://www.marinecorpstimes.com/article/20120907/NEWS/209070313/3-vehicles-contend-replace-Marines-Humvees

[29] Military pictures, “Army-tank”, Depositphotos, [Cited 04/20/2014]; Available from: http://www.desktopexchange.net/plog-content/images/military-pictures/tank-wallpapers/army-tank.jpg

[30] M. Meyers and K. Chawla, “Mechanical behavior of materials”, *Cambridge University Press*, Cambridge, United Kingdom, 2nd edition, pp25-43, 2009.

[31] W. D. Callister, “Materials science and engineering”, *J. Wiley & Sons, Inc*, New York, 7th edition, pp577-584, 2007.

[32] G. B. Veeresh Kumar, C, S, P. Rao and N. Selvaraj, “Mechanical and tribological behavior of particulate reinforced aluminum metal matrix composites-a review”, *Journal of Minerals & Materials Characterization & Engineering*, **10**(1), pp59-91, 2011.

[33] S. C. Sharma, “The sliding wear behavior of Al6061-garnet particulate composites”, *wear*, **249**(12), pp1036-1045, 2001.

[34] B. Bhushan, “Wear mechanisms” In Modern tribology handbook, edited by K. Kato and K. Adachi, *CRC Press*, London, United Kingdom, 2001.

[35] J. G, Kaufman, “Introduction to aluminum alloys and tempers”, *ASM International*, Materials Park, Ohio, p12, 2000.

[36] V. Marinov, “Manufacturing technology”, [Cited 04/20/2014]; Available from: http://me.emu.edu.tr/majid/Powder%20Metallurgy/ME364_PM_process.pdf

[37] S. Lampman, “Compressibility and compactibility of metal powders”, *ASM International*, Materials Park, Ohio, pp302-309, 1998.

[38] E. L. Tobolski, “Macroindentation hardness testing”, *ASM International*, Materials Park, Ohio, pp203-220, 2000.

[39] J. M. Thompson and M. K. Thompson, “A proposal for the calculation of wear”, [Cited 04/20/2014]; Available from: http://www.ansys.com/staticassets/ANSYS/staticassets/resourcelibrary/confpaper/2006-Int-ANSYS-Conf-286.pdf

[40] Gamry Instruments, “Gamry instruments software tutorials and primers”, *Gamry Instrumrnt INC*, Warminster, Pennsylvania, pp2-8, 2005.

[41] W. J. Lorenz and F. Manfeld, “Determination of corrosion rates by electrochemical DC and AC methods”, *Corrosion Science*, **21**(9-10), pp647-672, 1981.

[42] M. G. Fontana and R. W. Staehle, “Advances in corrosion science and technology”, *Plenum Press*, **2**(1), pp35-48 1976.

[43] Annual book of ASTM Standards, “Standard practice for calculation of corrosion rates and related information from electrochemical measurements”, *ASTM*, West Conshohocken, Pennsylvania, pp32-38, 1994.

[44] D. G. Enos and L. L. Scribner, “The potentiodynamic polarization scan”, Solartron Instruments, *Technical Report 33*, Hampshire, United Kingdom, pp9-15, 1997.

[45] D. A. Jones, “Principles and prevention of corrosion”, *Prentice Hall*, New Jersey, 2nd edition, pp128-169, 1996.

[46] T. D. Burleigh, E. Ludwiczak and R. A. Petri, “Intergranular corrosion of an aluminum-magnesium-silicon-copper alloy”, *Corrosion Science*, **51**(1), pp50-55, 1995.

[47] C. Vargel, M. Jacques and M. P. Schmidt, ″Corrosion of aluminum″, *Elsevier Science*, Boston, pp23-69, 2004.

[48] Galvele and De Micheli, “Mechanism of intergranular corrosion of Al-Cu alloys”, *Corrosion Science*, **10**(11), pp795-807, 1970.

[49] N. P. Suh, “The delamination theory of wear”, *Wear*, **25**(1), pp111-124, 1973.